General Disclaimer

One or more of the Following Statements may affect this Document

- This document has been reproduced from the best copy furnished by the organizational source. It is being released in the interest of making available as much information as possible.

- This document may contain data, which exceeds the sheet parameters. It was furnished in this condition by the organizational source and is the best copy available.

- This document may contain tone-on-tone or color graphs, charts and/or pictures, which have been reproduced in black and white.

- This document is paginated as submitted by the original source.

- Portions of this document are not fully legible due to the historical nature of some of the material. However, it is the best reproduction available from the original submission.

Produced by the NASA Center for Aerospace Information (CASI)

E77-10059

NASA

Final Report

INVESTIGATION OF SPATIAL MISREGISTRATION EFFECTS IN MULTISPECTRAL SCANNER DATA

W.A. MALILA, J.M. GLEASON, AND R.C. CICONE
Infrared and Optics Division

MAY 1976

Prepared for

NATIONAL AERONAUTICS AND SPACE ADMINISTRATION

∑ ENVIRONMENTAL RESEARCH INSTITUTE OF MICHIGAN

E77-10059

NASA

Final Report

INVESTIGATION OF SPATIAL MISREGISTRATION EFFECTS IN MULTISPECTRAL SCANNER DATA

W.A. MALILA, J.M. GLEASON, AND R.C. CICONE
Infrared and Optics Division

MAY 1976

Prepared for

NATIONAL AERONAUTICS AND SPACE ADMINISTRATION

ENVIRONMENTAL

RESEARCH INSTITUTE OF MICHIGAN

FORMERLY WILLOW RUN LABORATORIES, THE UNIVERSITY OF MICHIGAN
BOX 618 • ANN ARBOR • MICHIGAN 48107

1. Report No. NASA CR— ERIM 109600-68-F	2. Government Accession No.	3. Recipient's Catalog No.
4. Title and Subtitle Investigation of Spatial Misregistration Effects in Multispectral Scanner Data		5. Report Date May 1976
		6. Performing Organization Code
7. Author(s) W. A. Malila, J. M. Gleason, R. C. Cicone		8. Performing Organization Report No. 109600-68-F
9. Performing Organization Name and Address Environmental Research Institute of Michigan Infrared & Optics Divsion P. O. Box 618 Ann Arbor, Michigan 48107		10. Work Unit No. Task 13
		11. Contract or Grant No. NAS9-14123
12. Sponsoring Agency Name and Address National Aeronautics & Space Administration Johnson Space Center Houston, Texas 77058		13. Type of Report and Period Covered Final Technical Report May 15, 1975 through May 14, 1976
		14. Sponsoring Agency Code

15. Supplementary Notes

16. Abstract

Spatial misregistration in multitemporal Landsat multispectral scanner data can potentially degrade the performance of recognition processors operating on such data. The major objective of this investigation was to evaluate the effects of spatial misregistration on recognition performance. This objective could not be achieved, however, because the required data were not delivered as expected. Nevertheless, some useful analyses were carried out.

A model for estimating the expected proportion of multiclass pixels in a scene was generalized and extended to include misregistration effects. Another substantial effort was the development of a simulation model to generate signatures to represent the distributions of signals from misregistered multiclass pixels, based on single-class signatures.

Spatial misregistration causes an increase in the proportion of multiclass pixels in a scene and a decorrelation between signals in misregistered data channels. The multiclass pixel proportion estimation model indicated that that this proportion is strongly dependent on the pixel perimeter and on the ratio of the total perimeter of the fields in the scene to the area of the scene. Test results indicated that expected values computed with this model were similar to empirical measurements made of this proportion in four LACIE data segments.

The increased proportion of multiclass pixels due to misregistration results in fewer single-class pixels being available for training and recognition. Chances for recognition errors and crop area estimation biases are thus increased. Other

17. Key Words Multispectral Scanner Spatial Registration Data Processing Simulation Model	18. Distribution Statement Initial distribution is listed at the end of this document.

19. Security Classif. (of this report) Unclassified	20. Security Classif. (of this page) Unclassified	21. No. of Pages ix + 80	22. Price

16. Abstract (Continued)

simulation studies have shown misregistration effects on recognition accuracy to be negligible for single-class pixels but much more substantial for multiclass pixels, resulting in crop area estimation biases.

FORMERLY WILLOW RUN LABORATORIES, THE UNIVERSITY OF MICHIGAN

PREFACE

This document reports processing and analysis efforts on one task
of a comprehensive and continuing program of research in multispectral
remote sensing of the environment. The research is being carried out
for NASA's Lyndon B. Johnson Space Center, Houston, Texas, by the
Environmental Research Institute of Michigan (ERIM). The basic objec-
tive of this program is to develop remote sensing as a practical tool
for obtaining extensive environmental information quickly and economi-
cally.

The specific focus of the work reported herein was an investiga-
tion of the effects of spatial misregistration on one's ability to
extract information from multispectral scanner data, especially for
agricultural inventories.

The research covered in this report was performed under Contract
NAS9-14123 during the period 15 May 1975 to 14 May 1976. Dr. Andrew
Potter (TF3) served as the NASA Contract Technical Monitor. At ERIM,
work was performed within the Infrared and Optics Division, headed by
Richard R. Legault, Vice-President of ERIM, in the Information Systems
and Analysis Department, headed by Dr. Jon D. Erickson. Mr. Richard
F. Nalepka, Head of the Multispectral Analysis Section served as
Principal Investigator.

The authors wish to acknowledge the assistance of other members
of the ERIM staff in addition to those cited above. Dr. R. B. Crane
suggested and consulted on the derivation of the signature simulation
model (App. II) and the analysis of the special two-distribution case
(App. I) which were carried out by R. Cicone. Dr. H. M. Horwitz
derived the generalized procedure for estimating the expected number
of boundary pixels in a scene (Sec. 4.1); the extension to misregi-
stered data (Sec. 4.2) was by J. Gleason and W. Malila. Typing of
this report and earlier materials was performed ably by Miss. D.
Dickerson.

CONTENTS

PRECEDING PAGE BLANK NOT FILMED   PAGE INTENTIONALLY BLANK

CONTENTS (CONT.)

Page

FIGURES

FIGURES (Continued)

TABLES

1
SUMMARY, CONCLUSIONS, AND RECOMMENDATIONS

Spatial misregistration in multitemporal LANDSAT multispectral scanner data can potentially degrade the performance of recognition processors operating on such data for applications like LACIE, the Large Area Crop Inventory Experiment. The major objective of this investigation was to evaluate the effects of spatial misregistration on recognition performance. The major effort planned for this investigation could not be carried out because the prime requisite data, accurately registered LANDSAT multitemporal data sets, were not delivered as expected. The sliding delivery schedule and high priorities on efforts for other tasks of this contract also resulted in a reduction of resources allocated for this particular investigation. Nevertheless, some useful analyses were carried out.

A model for estimating the number of multiclass pixels in the scene, i.e., pixels which represent more than one ground cover class, such as along field boundaries, was generalized and extended to include misregistration effects. These models apply to situations where the pixel dimensions are small in comparison to field dimensions. A series of parametric graphs was then generated to portray the influence of the key variables. Another substantial effort was the development of a simulation model to generate signatures (mean vectors and variance-covariance matrices) to represent the distributions of signals from misregistered multiclass pixels, based on single-class signatures extracted from data sets of interest. Also, computer programs to induce misregistration by fixed amounts in accurately registered data were written, although not used, and the between-channel misregistration in two single-time LACIE segments of LANDSAT data was measured.

1.1 CONCLUSIONS

(1) The two major direct effects of spatial misregistration on multitemporal data are:

1

(a) an increase in the percentage of pixels that are multi-class pixels and

(b) a decorrelation of signals in spatially misregistered data.

(2) Use of the method developed to estimate the expected proportion of multiclass pixels in both registered and misregistered data showed that:

(a) Estimates obtained using the method were reasonably similar to empirical measurements for four LACIE intensive test sites in Kansas.

(b) The proportion of multiclass pixels in a scene is proportional in an approximate sense to the perimeter of the pixel and to the ratio of the total perimeter of the fields in the scene to the area of the scene.

(c) For the four intensive test sites, the perimeter-to-area ratio for each site, plotted against the average field size within each, produced a smooth curve. This would indicate that the perimeter-to-area ratio, and consequently the expected proportion of multiclass pixels, can be determined in an approximate sense directly from the average field size for any site in the Kansas region or any other region with similar field patterns.

(d) For a simulated, rectangular field pattern, the expected proportion of multiclass pixels is most sensitive to variations in the size of the fields and their aspect ratio when these quantities are small.

(e) For the simulated field pattern, the expected proportion of multiclass pixels decreases as the size of the fields increases and as their shape approaches that of a square.

(f) Misregistration increases the proportion of multiclass pixels, dependent on the magnitude and direction of the misregistration

2

and the size of the pixel; this increase is equivalent to the effect of using a larger pixel size.

(3)   The increased percentage of multiclass pixels present in a misregistered scene has the following effects on computer recognition processing and performance:

(a)   Fewer single-class pixels are available for training, and more stringent inset requirements must be placed on the specification of single-class training fields to insure that multiclass pixels are excluded.

(b)   Fewer single-class pixels are available for recognition and chances for recognition errors and crop area estimation biases among multiclass pixels are increased.   Quantification of these effects for LACIE data was an unachieved objective of this investigation due to the unavailability of the requisite data.   However, the simulation model developed was used to demonstrate such effects for SKYLAB S-192 data from a corn-soybean agricultural scene under another investigation.

(4)   The reduction of correlation between misregistered data channels would have the following effects on recognition processing and performance:

(a)   For single-class pixels, although not intuitively obvious, misregistration might possibly decrease probability of misclassification; other simulation studies have shown misregistration effects on single-class pixels to be negligible.

(b)   For multiclass pixels, however, misregistration effects have been shown to be substantial in other studies, but the effects of different proportions of materials present and decreased correlation between misregistered channels are difficult to separate; the comments of (3)(b) apply here as well.

(5)   No evidence of significant amounts of between-channel misregistration in single-pass LANDSAT data was found in the two data segments analyzed.

3

1.2 RECOMMENDATIONS

Although the contract effort could not be completed as originally planned, the work which has been performed and reported herein has yielded both additional insight into the overall difficulties attributable to misregistration and tools with which to further evaluate its effects. On this basis, the following recommendations are made:

(1) The effects of misregistration on recognition accuracy and proportion estimation accuracy should be quantified more fully for the LACIE application and other applications.

(a) Methods using the simulation models developed in the reported effort could be investigated and used to address this question in a general sense but yet with primary emphasis on the LACIE application. Clearly, the effects of misregistration on recognition accuracy and proportion estimation accuracy depend in large part on the field pattern, the signatures of the various crop categories, and the true crop proportions in the particular scene analyzed. The models developed would allow the expected proportions of multiclass and single-class pixels to be determined as a function of the amount of misregistration for typical LACIE field patterns. The signatures of these multiclass pixels could then be simulated from typical single-class LACIE crop signatures. With these and other tools, the effects of misregistration could be more thoroughly investigated than previously possible.

(b) The accurately registered LACIE multitemporal data sets that are now available should be used to evaluate the effects of misregistration on these specific data sets, as originally planned, for the dual purpose of obtaining quantitative results for specific data sets and verifying the accuracy of the simulation models.

(2) Additional investigation should be made of the ERIM method for estimating the expected proportion of multiclass pixels in a scene.

4

(a) Further efforts should be undertaken to evaluate its accuracy and utility.

(b) Tests should be conducted to determine if the perimeter-to-area ratio of a scene can be accurately related to the average field size within the scene in terms of the standard agricultural practices used in a given geographical area. If such a relationship can be established, the only information necessary to estimate the expected proportion of multiclass pixels in a particular scene, by the approximate ERIM method, is the average field size in that scene.

(c) The method should be extended further to account for the effects of both pixel ground area overlap and simultaneous mis-registration along and between scan lines on the expected proportion of multiclass pixels in a scene.

2

INTRODUCTION

One of the major uses being developed for LANDSAT multispectral scanner data is for the inventory of agricultural crops and production forecasting, e.g., LACIE, the Large Area Crop Inventory Experiment. Average misregistrations of nearly one pixel have been reported in LACIE multitemporal data [1]. The major objective of the effort reported herein was to evaluate the effects of spatial misregistration on recognition performance of processors operating on multitemporal LANDSAT data.

Spatial misregistration produces two effects in multitemporal data which potentially can degrade recognition performance. First, it increases the proportion of scene multiclass pixels which represent signals from more than one class of ground cover (e.g., mixture pixels which occur at or near field boundaries). This increase in the proportion of multiclass pixels both reduces the availability of pure field-center (single-class) pixels for training and increases the likelihood of recognition errors in the scene, as will be shown in the analyses that follow. The second effect of misregistration is on single-class pixels where it reduces the correlation between signals in the channels that are out of registration.

Initial work on this effort was begun and reported last year [2]. A simple model was developed to simulate signatures from misregistered pixels that contained mixtures of two materials. Initial calculations were made using CITARS data signatures to predict the effects of such misregistration on recognition performance, and it was shown to potentially cause substantial degradation.

The signature simulation model was generalized and improved more recently under joint support of this contract and a Skylab investigation[*]

---

[*]Contract NAS9-13280 with NASA's Johnson Space Center, Houston, Texas; the final report is Ref. 3.

carried out at ERIM. Simulations of misregistration effects in single-pass Skylab S-192 multispectral scanner data were made using the improved model, analyzed, and reported in Ref. 3. In brief, it was found that (a) the availability of single-class (field-center) pixels was substantially reduced for small amounts (one pixel and even less) of misregistration, (b) classification accuracy for single-class pixels was not significantly affected by misregistration, (c) overestimates of the proportions of certain crops were linked directly to misregistration, and (d) overall classification accuracy was degraded by misregistration, bringing into question the common belief or tacit assumption that mixture pixels and misregistration effects produce compensating errors. Some of these topics are analyzed more fully in the current report.

3
APPROACH

The planned approach for this effort was to place heavy reliance on empirical simulations of misregistration to assess its effects on recognition performance. Multitemporal data sets registered by a state-of-the-art procedure were to have been deliberately misregistered by several different amounts and the effects on recognition performance determined. This empirical analysis was then to have been supported and extended by theoretical analyses using signature simulation models to combine and transform signatures extracted from the accurately registered data to simulate additional misregistration cases and conditions. Also, recognition results obtained from the accurately registered data were to have been compared with results obtained from data registered by the current LACIE procedure. Finally, of lowest priority, was to have been an assessment of the relationship between average field size and recognition performance in the presence of misregistration.

The first months of the effort were primarily involved with planning the empirical simulation experiment and developing computer programs to misregister the data. Also, development work was performed on the signature simulation models and, in the absence of the accurately registered data sets, some analysis of the joint effects of field size and misregistration was begun.

The date by which NASA expected to deliver to ERIM the accurately registered data sets was progressively delayed throughout the contract period with the end results being that the data were not delivered before this report was drafted and the primary efforts planned for this task could not be carried out. The combination of the sliding delivery schedule for the essential data and pressing priorities on other tasks resulted eventually in a reduction of resources allocated to this task and an inability to meet all task objectives. Nevertheless, some useful results were obtained and are reported in succeeding sections.

The influence of misregistration on the proportion of multiclass
pixels present in scenes was analyzed t'ieoretically through the develop-
ment of a model by which the expected proportion of multiclass pixels
in a scene could be estimated. Parameters in this model are the total
length of boundary in the scene, the number of nodes in the field
pattern, the pixel dimensions (rectangular), the total scene area, and
the amount of misregistration. A series of calculations and parametric
graphs were produced using the model to   esent the overall effects
and dependencies.

Both analytical and simulation techniques were developed to assess,
theoretically, the effects of misregistration on classification accu-
racy and proportion estimation. The basic computational tool intended
for use was a program to compute probabilities of detection and false
alarm based on signatures (mean vectors and variance-covariance matrices).
Thus, simulation models were developed to combine and transform single-
class signatures extracted from actual registered scanner data so they
would represent signal distributions from misregistered single-class
and multiclass pixels.

Five categories of pixels were identified for the analysis.
Four of these are illustrated in Fig. 1: (a) pure field-center
(single-class) pixels which remain single-class pixels when misregi-
stered; (b) single-class pixels for which those channels out of regi-
stration represent mixtures of two or more crop types; (c) mixture
pixels for which channels out of registration represent different
mixture proportions; and (d) mixture pixels for which those channels
out of registration again represent a single class. A fifth class,
(e), consists of multiclass pixels that due to misregistracion are
made up of field-center pixels from two or more different classes.
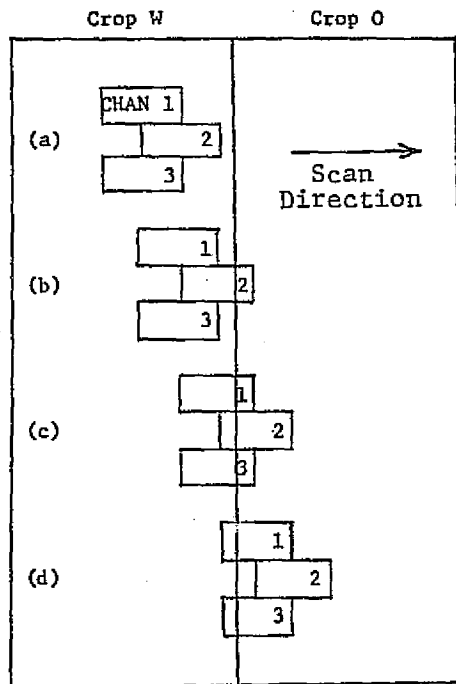
FIGURE 1. ILLUSTRATION OF FOUR CATEGORIES OF MISREGISTERED PIXELS.
(The three channels in each pixel are offset vertically
for clarity; Ch. 2 is misregistered by 1/2 pixel along
the scan line.)

4
INFLUENCE OF MISREGISTRATION ON THE PROPORTION
OF MULTICLASS PIXELS PRESENT

A significant effect of spatial misregistration, between two or more single-time data sets combined to form a multitemporal data set, is the potentially sizable reduction in the number of single-class pixels within the multitemporal data set from the number existing within any of the single-time data sets. Within a single-time data set (perfectly registered between channels), two types of pixels may exist: single-class or field-center pixels and multiclass or mixture pixels which cross field boundaries.

In a multitemporal data set formed from two or more perfectly registered single-time data sets, all pixels will be of these two types and exist in the same proportions as in the single-time data sets. If, however, the single-time data are misregistered, a new type of multiclass pixel will be created and add to the total number of multiclass pixels in the scene. A multiclass pixel which exists in misregistered multitemporal data has the characteristic that the proportions of its constituent classes differ between time periods and some of these constituents may even be different for the various time periods.

An algorithm for estimating the expected proportion of boundary pixels occurring in data obtained by a sensor with a square pixel from a scene consisting of a "quilt" pattern of rectangular fields had been developed previously by Gray and Duran [4]. Dr. H. M. Horwitz of ERIM has developed a more general and simpler algorithm for estimating the value of this same quantity, based upon an intermediate result in Barbier's solution of the Buffon needle problem [5]. The ERIM method allows both for scenes consisting of non-overlapping polygonal areas (i.e., is not limited to rectangles) and for a rectangular pixel shape. Sec. 4.1 presents the derivation of this new estimation procedure and

discusses it in some detail. In Sec. 4.2, this estimation procedure is extended to estimate the expected proportion of multiclass pixels in multitemporal data that contain misregistration. Finally, in Sec. 4.3, the models are applied. An estimate of the expected proportion of boundary pixels obtained by the ERIM method in each of four LACIE intensive test sites is compared to an actual measurement of this proportion obtained directly from the field pattern existing in the site. Also, a series of curves are presented, displaying the expected proportion of multiclass pixels determined by the ERIM method for both registered and misregistered multitemporal data containing fields of varying size and aspect ratio. Various pixel dimensions are also considered.

4.1 DERIVATION OF ERIM METHOD FOR ESTIMATING THE EXPECTED PROPORTION OF BOUNDARY PIXELS

Suppose that the scene S is filled by non-overlapping simple closed polygons as in Fig. 2, and that a rectangular grid G as illustrated in Fig. 3 is placed at random on the scene S. The width of each rectangle in the grid is w and its height is h; each rectangle corresponds to one pixel, where the pixels do not overlap. Grid rectangles which contain the boundary of any polygon in the configuration S are then multiclass boundary pixels. The number of these boundary pixels is defined as a random variable β.

To arrive at an approximation to $E(\beta)$, the expected value of β, certain preliminary results are required. Let γ denote the total number of crossings of lines in the configuration S with lines in the grid G. Then it follows from Ref. 5 that

$$E(\gamma) = \frac{2L}{\pi}\left(\frac{1}{h} + \frac{1}{w}\right) \tag{1}$$

where L is the sum of the lengths of all the lines in configuration S.
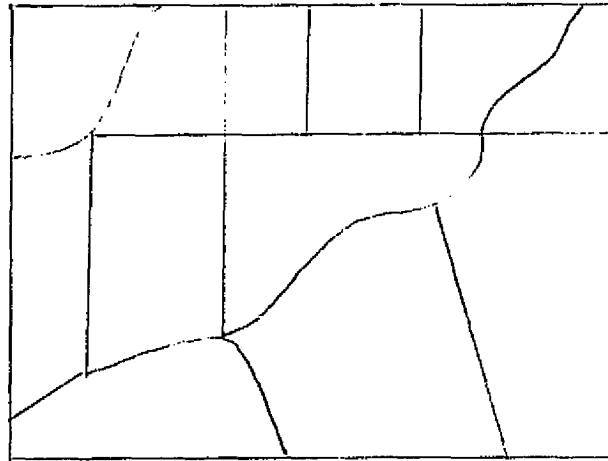
FIGURE 2.   TYPICAL SCENE CONFIGURATION
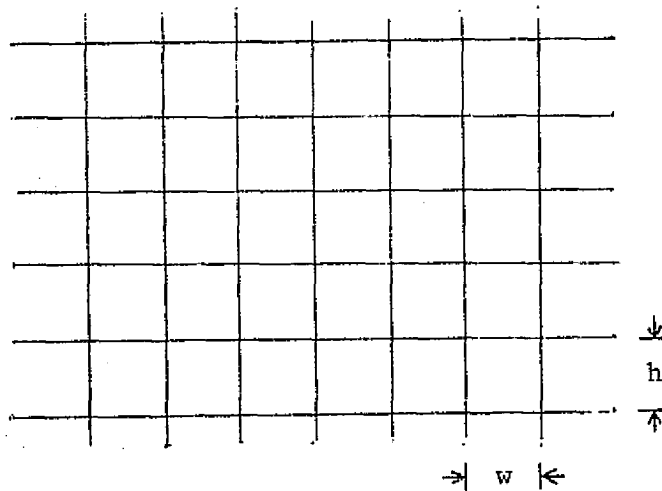
FIGURE 3.   RECTANGULAR PIXEL GRID

When the dimensions of the polygons forming configuration S are large with respect to the grid parameters h and w, most of the boundary pixels will be of two types: (a) those pixels whose edges have exactly two intersections with lines of configuration S and (b) those pixels which contain a single node of configuration S. (A node is defined as a point where at least three polygons meet.) Clearly, these two types of boundary pixels are disjoint classes. Assuming that the number of boundary pixels of types other than these two are negligible, $E(\beta)$ may then be related to $E(\gamma)$. Let a_1, a_2,...a_r denote all the nodes in S, and let $\upsilon(a_i)$ denote the number of polygons meeting at node a_i. Setting

$$s = \sum_{i=1}^{r} \upsilon(a_i) \tag{2}$$

it can be shown by elementary counting arguments that

$$E(\beta) = E(\gamma) - \left(\frac{s}{2} - r\right) \tag{3}$$

To prevent an overestimate of the number of boundary pixels due to the overhang of the grid on the scene, a factor

$$\frac{B}{\pi}\left(\frac{1}{h} + \frac{1}{w}\right) \tag{4}$$

must be subtracted from (3), where B is the perimeter of the scene. The resulting expression obtained then is

$$E(\beta) = \frac{(2L - B)}{\pi}\left(\frac{1}{h} + \frac{1}{w}\right) - \left(\frac{s}{2} - r\right) \tag{5}$$

The expected proportion R of boundary pixels in the scene S is approximated by

$$R = \frac{E(\beta)}{N} \tag{6a}$$

14

where N is the number of pixels in the scene, or

$$R = \frac{E(\beta) \cdot h \cdot w}{A} \qquad (6b)$$

where $A = N \cdot (hw)$ is the area of the scene. It should be noted that when nodes in a scene are determined, the region exterior to S is counted as a polygon. For example, in Fig. 4, a_1, a_2, a_3, a_4 and a_5 are the only nodes and $\upsilon(a_i) = 3$, $1 \le i \le 4$, and $\upsilon(a_5) = 4$.

When w and/or h are sufficiently small, the first term in the right-hand side of Eq. (5) increases and becomes dominant over the second term which remains constant. Substituting this first term into Eq. (6), the following additional approximations can be made:

$$R \approx \frac{(2L - B)}{\pi N} \left(\frac{h + w}{hw} \right) \qquad (7)$$

or

$$R \approx \frac{P}{\pi A} (h + w) \qquad (8)$$

where P is the sum of the perimeters of all polygons in configuration S and is defined as

$$P = 2L - B \qquad (9)$$

Thus, in this limiting case, the expected proportion of boundary pixels is proportional to the ratio of the perimeter of the scene polygons to the area of the scene or to the ratio of the perimeter, $2(h + w)$, of the pixel to the area of the pixel.
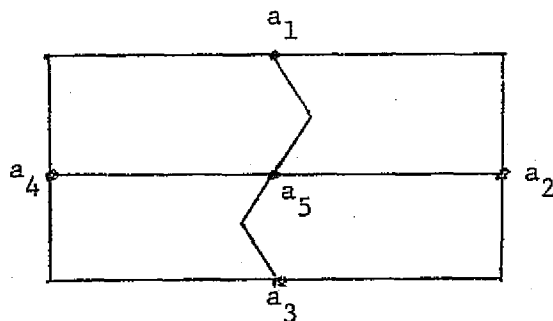
FIGURE 4. DETERMINATION OF SCENE NODES

4.2 EXPECTED PROPORTION OF MULTICLASS PIXELS IN MISREGISTERED MULTITEMPORAL DATA

In the previous section a method was derived for estimating the expected proportion of boundary or multiclass pixels in single-time data sets or in perfectly registered multitemporal data sets. In this section, that method will be extended to obtain estimates of the expected proportion of multiclass pixels in misregistered multitemporal data. The misregistration in this data will be assumed to occur with a subset of data channels being misregistered with respect to the remaining channels and will be restricted to one pixel or less in magnitude either along the scan line or perpendicular to it. The dimensions of the pixel will be assumed to be small enough in comparison to the size of the fields in the scene that, essentially, all multiclass pixels which exist in the perfectly registered data are of the type that have exactly two intersections with the field boundaries. The assumption will also be made that the pixel dimensions are small enough that the boundary segment, intersecting the edges of each multiclass pixel in the registered data, can be considered as a straight line segment. No restrictions will be made on the shape of the fields which may exist in the scene; the only assumption which will be made is that the straight line boundary segments within boundary pixels are randomly oriented and distributed over those pixels.

Given that a certain proportion of multiclass pixels exists in perfectly registered multitemporal data, the effects of misregistering a subset of channels with respect to the remaining channels will be to increase the proportion of multiclass pixels. It should be recalled that the multiclass pixels in misregistered data will consist of different proportions of ground classes in the two subsets of channels and may even consist of different sets of ground classes in those channels. Figure 5 illustrates three cases for two adjacent pixels along a scan line and a misregistration between channels of a distance Δw along the scan line. In this figure the solid lines represent the

16

Boundary Segment

(a)   (b)   (c)
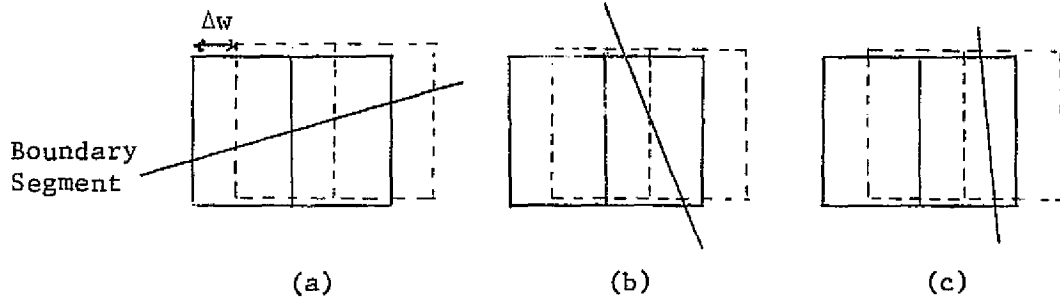
FIGURE 5.   EFFECTS OF MISREGISTRATION ALONG THE SCAN LINE

$\alpha_T(x,y)$

α_L

(x,y)

Boundary Segment

$\alpha_B(x,y)$
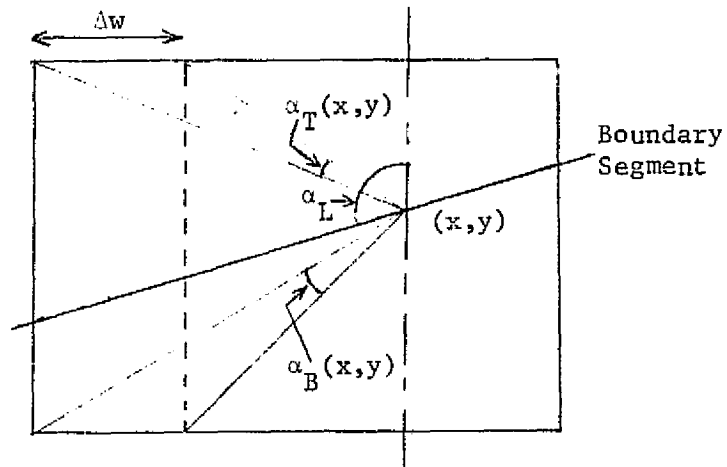
FIGURE 6.   BOUNDARY LINE SEGMENT ORIENTATION
            WITHIN A PIXEL

17

position of the pixels in one subset of channels and the dashed lines
represent the position of the pixels in the remaining subset of chan-
nels misregistered with respect to the first subset. If the two sub-
sets of channels were perfectly registered the solid line would indi-
cate their position and in each case the right-hand pixel is a multi-
class pixel, while only in case (a) is the left hand pixel also a
multiclass pixel. In the presence of misregistration, the right-hand
pixel is still a multiclass pixel in all cases but now the left-hand
pixel in case (b) is also a multiclass pixel whereas in the absence of
misregistration it was not. The effect of misregistration (e.g., to
the right) along the scan line in multitemporal data is to create new
multiclass pixels whenever both (a) a pixel which is not itself a
multiclass pixel exists immediately to the left of one which is, in the
registered data, and (b) the boundary segment within that pixel inter-
sects the top or bottom edge of the pixel within a distance Δw from
its left edge. Misregistration between scan lines results in a similar
increase in the expected proportion of multiclass pixels.

The proportion of multiclass pixels in perfectly registered data
may be determined by the method derived in the previous section and
will be denoted by R. The proportion of multiclass pixels in multi-
temporal data which is misregistered by a distance Δw along the scan
line will be denoted by $R'(\Delta w)$. The proportion of multiclass pixels
in the misregistered data can then be expressed as:

$$R'(\Delta w) = R[1 + p_c(\Delta w)] \tag{10}$$

where the quantity $p_c(\Delta w)$ is the probability that a line, randomly
oriented about a point (x,y) chosen at random within a pixel, will
intersect either the top or bottom edge of the pixel within a distance
Δw from its left edge. Figure 6 illustrates a line segment through
the point (x,y) and making an angle α_L with the vertical line drawn
through the point (x,y). In this figure, the angles $\alpha_T(x,y)$ and $\alpha_B(x,y)$

18

represent the range of angles over which the line segment will inter-
sect the regions of interest along the top and bottom edges of the
pixel, respectively. The angle α_L will be assumed to be uniformly
distributed over an angle of π radians to the left of the vertical
line and the point (x,y) will be assumed to be uniformly distributed
over the pixel interior. In App. III, $p_c(\Delta w)$ is derived analytically
with the result that

$$p_c(\Delta w) = \frac{h}{2\pi w} \ln \left(\frac{1 + \frac{(w-\Delta w)^2}{h^2}}{1 + \frac{w^2}{h^2}} \right) + \frac{w}{2\pi h} \ln \left(1 + \frac{h^2}{w^2} \right)$$

$$- \frac{(w-\Delta w)^2}{2\pi hw} \ln \left(1 + \frac{h^2}{(w-\Delta w)^2} \right) + \frac{2}{\pi} \cot^{-1} \left(\frac{h}{w} \right) - \frac{2(w-\Delta w)}{\pi w} \cot^{-1} \left(\frac{h}{w-\Delta w} \right)$$

or letting

$$r = \frac{h}{w}$$

be defined as the aspect ratio of the pixel, and

$$m_w = \frac{\Delta w}{w}$$

be defined as the fractional pixel misregistration along the scan
line, $p_c(\Delta w)$ can be written as

$$p_c(\Delta w) = p_c(m_w) = \frac{r}{2\pi} \ln \left(\frac{r^2 + (1-m_w)^2}{r^2 + 1} \right) + \frac{1}{2\pi r} \ln (1 + r^2)$$

$$- \frac{(1-m_w)^2}{2\pi r} \ln \left(1 + \frac{r^2}{(1-m_w)^2} \right) + \frac{2}{\pi} \cot^{-1}(r) - \frac{2(1-m_w)}{\pi} \cot^{-1} \left(\frac{r}{1-m_w} \right)$$

and $R'(\Delta w)$ can be written as

$$
R'(\Delta w) = R'(m_w) = R \left[1 + \frac{r}{2\pi} \ln \left(\frac{r^2 + (1-m_w)^2}{r^2 + 1} \right) + \frac{1}{2\pi r} \ln (1 + r^2) \right.
$$

$$
\left. - \frac{(1-m_w)^2}{2\pi r} \ln \left(1 + \frac{r^2}{(1-m_w)^2} \right) + \frac{2}{\pi} \cot^{-1}(r) - \frac{2(1-m_w)}{\pi} \cot^{-1} \left(\frac{r}{1-m_w} \right) \right] \quad (11)
$$

Using similar arguments the expected proportion of multiclass pixels in data which contains misregistration of distance Δh between scan lines can be written as

$$
R'(\Delta h) = R'(m_h) = R \left[1 + \frac{1}{2\pi r} \ln \left(\frac{1 + r^2(1-m_h)^2}{1 + r^2} \right) + \frac{r}{2\pi} \ln \left(1 + \frac{1}{r^2} \right) \right.
$$

$$
\left. - \frac{r(1-m_h)^2}{2\pi} \ln \left(1 + \frac{1}{r^2(1-m_h)^2} \right) + \frac{2}{\pi} \cot^{-1} \left(\frac{1}{r} \right) - \frac{2(1-m_h)}{\pi} \cot^{-1} \left(\frac{1}{r(1-m_h)} \right) \right]
$$

$$
(12)
$$

where, as before

$$
r = \frac{h}{w}
$$

is the pixel aspect ratio, and

$$
m_h = \frac{\Delta h}{h}
$$

is defined as the fractional pixel misregistration between scan lines.

ERIM

4.3 APPLICATION OF ESTIMATION PROCEDURES FOR EXPECTED PROPORTION
     OF MULTICLASS PIXELS

The procedures developed in the previous sections will be employed
in this section to estimate the expected proportion of multiclass pixels
in both registered and misregistered multitemporal data from scenes
containing either actual or simulated field patterns. The actual scene
patterns will correspond to those existing in four LACIE intensive test
sites in the Kansas region. Estimates for the field patterns in each
of these sites will be made, assuming perfectly registered LANDSAT
data. These expected values will be compared with measurements
obtained by an empirical procedure from one data set for each site.

Next, simplifying assumptions will be made in the model to allow
estimates to be obtained in terms of the perimeter-to-area ratio of
scenes containing the simulated field patterns.

These simulated field patterns will consist of a regular arrange-
ment of identical rectangular fields of varying size and aspect ratio.
Curves will be presented, illustrating the dependence of the propor-
tions on the dimensions of the pixel, the size and aspect ratio of the
simulated fields, and the amount and direction of misregistration in
the data. In addition, relationships between average field size and
perimeter-to-area ratio will be examined for the Kansas sites.

Theoretical estimates of the expected proportion of multiclass
pixels in perfectly registered multitemporal data were made for four
LACIE intensive test sites in Kansas: Finney, Ellis, Morton, and
Saline. A computer program was written to compute the quantities
required in Eq. (5) from the vertices of a set of polygons describing
the field pattern in each site. The ground-equivalent pixel dimensions
were chosen to pertain to LANDSAT data; the height of the pixel was set
to 79 m and its width to 57 m.

This width represents the separation between LANDSAT data values
along the scan line. However, there is an overlapping of the ground
areas corresponding to adjacent LANDSAT pixels because the actual width

of the LANDSAT spatial resolution element is 79 m. The theoretical
methods developed in this report do not currently incorporate terms
to directly account for increases in the proportion of multiclass
pixels due to such overlapping resolution elements.

The empirical procedure relied on a determination of the number
of field-center pixels in an actual LANDSAT data set for each site,
again neglecting the overlap present along the scan lines. This num-
ber was subtracted from the total number of pixels in each site and
divided by this same total to obtain the desired proportion. Field-
center pixels were defined as those pixels with centers more than one-
half pixel distance from the edge of each field, as determined from
the set of polygons describing the field pattern. Table I summarizes
the expected proportions computed using the ERIM theoretical method
and the corresponding empirical measurements. The average size of the
fields in each site and the ratio (P/A) of the total perimeter P of all
fields to the area A of each site are also listed.

This test is hardly sufficient to allow definitive conclusions
to be drawn about the accuracy of the theoretical method, but the
results indicate that the theoretical expected values and the corre-
sponding empirical measurements of multiclass pixel percentages are
reasonably similar. The average of the absolute value of the difference
between the two values is approximately 6%, with the average difference
being 2% greater for the empirical measurement. Direct comparisons of
these two quantities must be made with caution since the theoretical
estimate applies to the expected value for all possible orientations
of the sampling grid on the scene pattern, whereas the empirical
measurement is for just one of these possible orientations. Further-
more, the true proportions of multiclass pixels are not known exactly
and the empirical measurements are believed to be slightly biased
(toward higher proportions) due to the way field vertices were defined,

TABLE I. PERCENTAGES OF MULTICLASS PIXELS AND OTHER
CHARACTERISTICS OF FOUR KANSAS
INTENSIVE TEST SITES

Intensive Test Site	Percentage of Multiclass Pixels		Average Field Size (Acres)	$\frac{P}{A}$
	Expected Percentage Using ERIM Theoretical Method	Empirical Measurement		
Ellis	48%	41%	29	0.012
Saline	43%	51%	34	0.011
Finney	41%	40%	37	0.010
Morton	23%	30%	78	0.005

i.e., there was a tendency to place each vertex slightly toward the
field center to insure good definition of field-center pixels. Also,
the polygons were defined for other uses at different times by different
individuals for the various sites. More precise and controlled experi-
ments will have to be conducted before this accuracy can be better
evaluated.

Additional analysis of the results presented in Table I reveals
that a strong positive correlation exists between the P/A ratio and
the estimate obtained by the ERIM theoretical method. The average
field size is negatively correlated with the P/A ratio, resulting in
an increased expected proportion of boundary pixels as the average
field size decreases.

The simulated field pattern consists of a large number of identi-
cal rectangular fields, a small section of which is illustrated in
Fig. 7. The dimensions of each field are C x D, with aspect ratio F,
defined as

$$F = C/D$$

and area A_F, defined as

$$A_F = C \cdot D.$$

Assuming that the scene contains T such fields on a side, and that the
pixel dimensions are small with respect to the size of each field, the
expected proportion R, of multiclass pixels in a registered data set
obtained from the scene, is determined from Eq. (8) as:

$$R = \frac{2T^2(C + D)}{\pi T^2 A_F} (h + w)$$

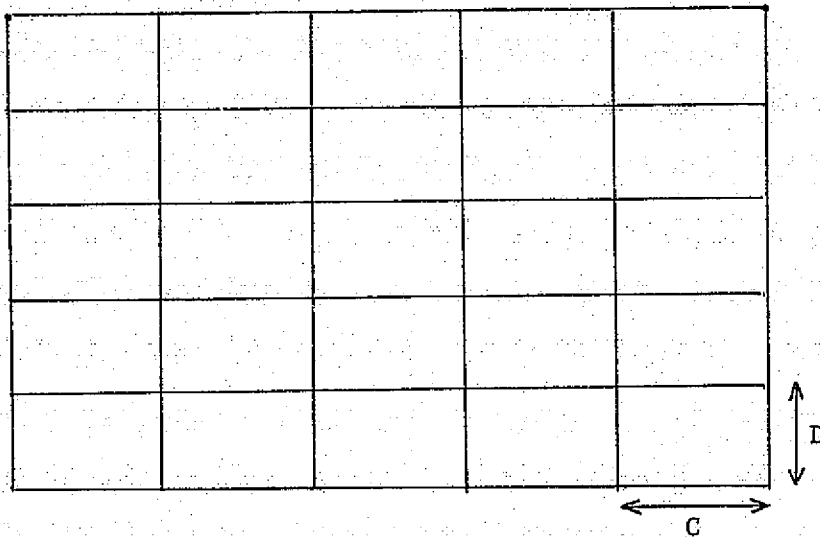$$= \frac{P}{\pi A} (h + w) \tag{13}$$

24

FIGURE 7. SIMULATED FIELD PATTERN

where the ratio P/A is given by

$$P/A = \frac{2T^2(C + D)}{T^2 A_F} = \frac{2(C + D)}{A_F}$$

Thus, the perimeter-to-area ratio of the entire scene is identically
equal to the perimeter-to-area ratio of each simulated field. Eq. (13)
expresses R in terms of the perimeter-to-area ratio of the scene and
the perimeter of the pixel.

Figs. 8-10 present curves illustrating the dependence of the
expected proportion of multiclass pixels on the dimensions of the
pixel, the size and aspect ratio of the simulated fields and the amount
and direction of misregistration in the data. Eq. (13) was used to esti-
mate the expected proportion of multiclass pixels in registered data
obtained from the simulated scenes and Eqs. (11) and (12) were used to
extend these estimates to account for misregistration. Each figure
contains two sets of curves. The top set represents the expected pro-
portion of multiclass pixels as a function of the P/A ratio of the
scene for various pixel dimensions or amounts of misregistration.
The bottom set of curves represents the P/A ratio of the scene plotted
against the field size of the simulated fields for several field aspect
ratios. In addition to these curves for the simulated field patterns,
a curve is also drawn through the points corresponding to the P/A
ratios and average field sizes determined for the four intensive test
sites. Since the top set of curves are related to the field pattern
only through the P/A ratio, the approximate expected proportion of
multiclass pixels in each intensive test site can then be determined
directly from these figures for the pixel dimensions and amounts of
misregistration represented by the top set of curves. Furthermore,
assuming that the curve drawn through these points is representative
of the relationship between average field size and P/A ratio for the
Kansas area, estimates may be obtained directly from these figures for
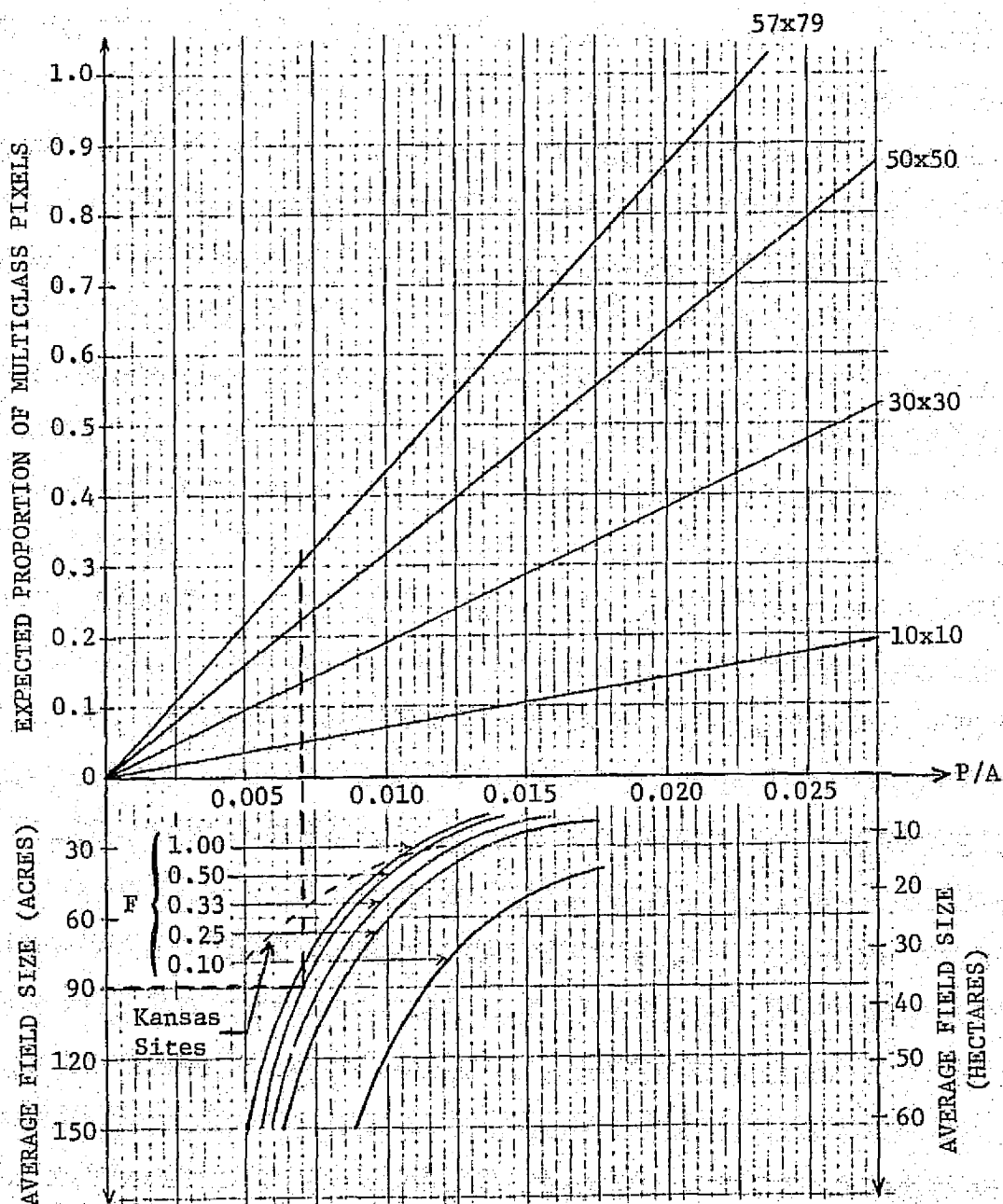
Notes: P/A = Perimeter-to-area ratio of scene.
F = Aspect ratio of rectangular fields
in simulated scene.

FIGURE 8.   EFFECTS OF PIXEL SIZE ON EXPECTED PROPORTION
OF MULTICLASS PIXELS
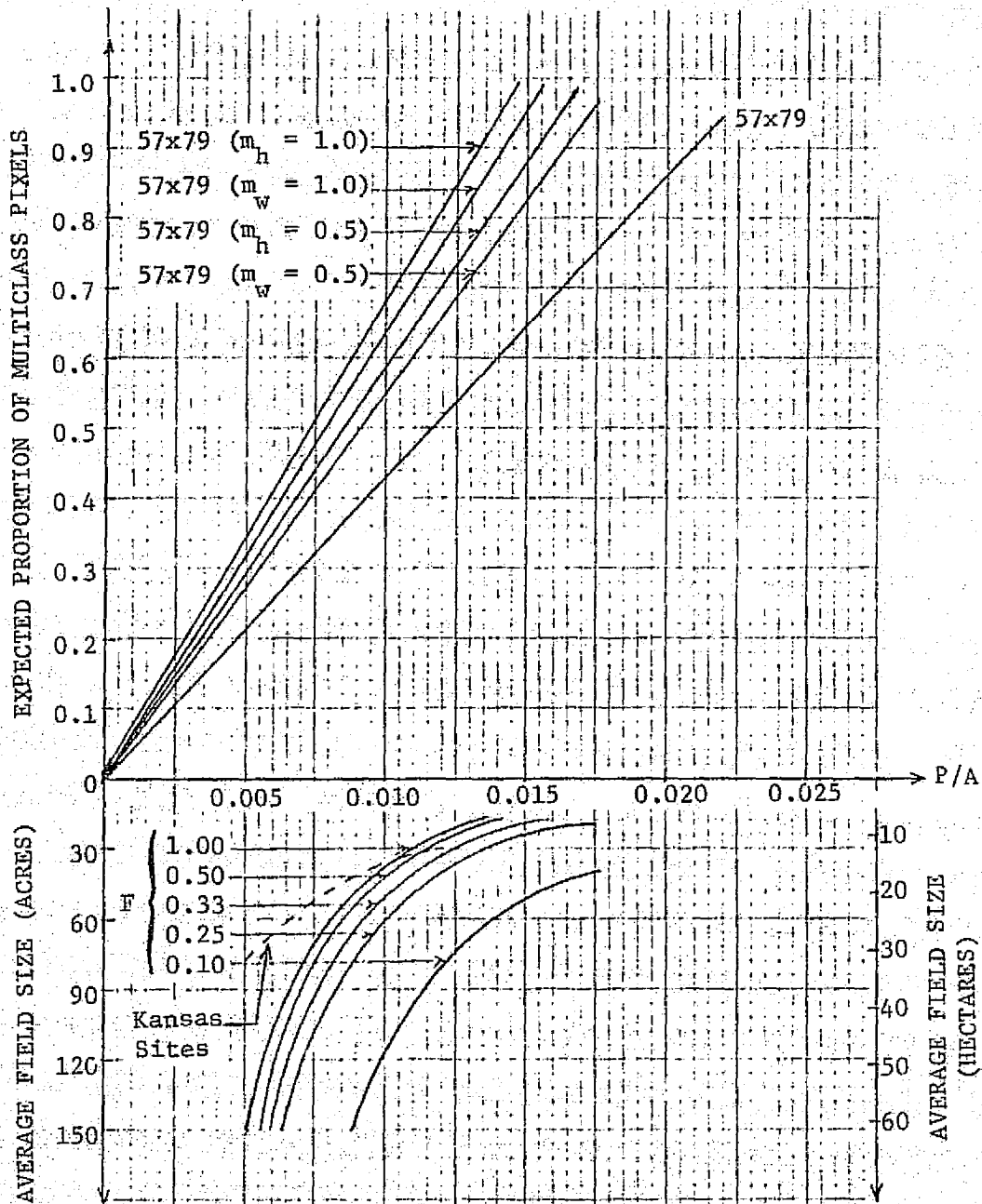
27

Notes: P/A = Perimeter-to-area ratio of scene.
F = Aspect ratio of rectangular fields
in simulated scene.

FIGURE 9. EFFECTS OF MISREGISTRATION ON EXPECTED PROPORTION
OF MULTICLASS PIXELS FOR 57x79 m PIXEL SIZE,
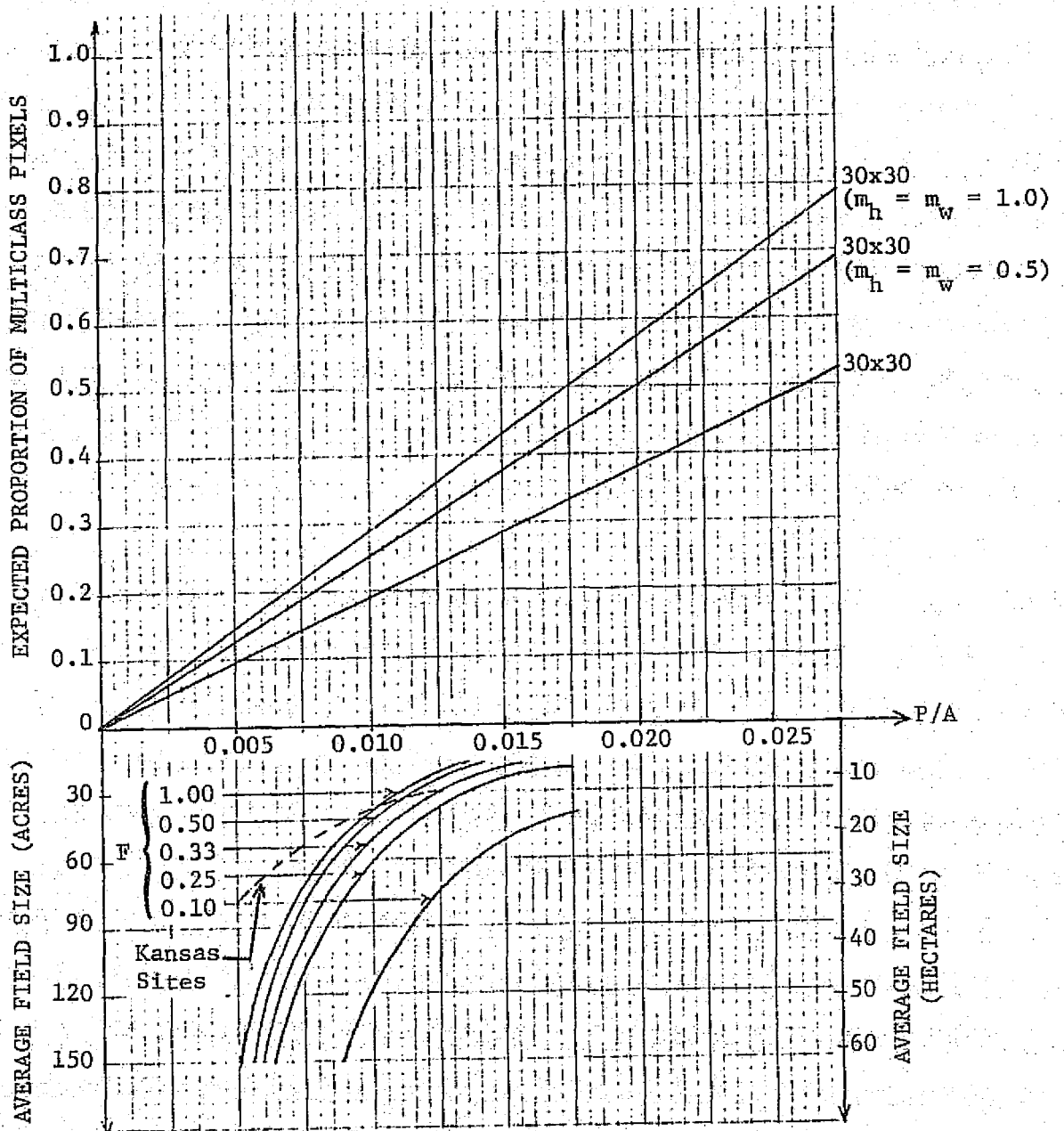NEGLECTING PIXEL OVERLAP

28

Notes: P/A = Perimeter-to-area ratio of scene.

F = Aspect ratio of rectangular fields
in simulated scene.

FIGURE 10. EFFECTS OF MISREGISTRATION ON EXPECTED PROPORTION
OF MULTICLASS PIXELS FOR 30x30 m PIXEL SIZE

any other site in the Kansas area, given the average size of the fields in the site. In the same manner, these curves could be used for other regions of the U.S. or world with similar field patterns.

In Fig. 8, the expected proportion of multiclass pixels in perfectly registered data is plotted in the top of the figure for four sets of pixel dimensions. The intersection of the dashed line with each of the curves in the top part of the figure indicates the expected proportion of multiclass pixels obtained for each set of pixel dimensions from a simulated scene containing 90-acre fields with a 0.5 aspect ratio. One point to note, which actually pertains to all three figures, is the greater sensitivity of the expected proportion of multiclass pixels to variations in the average field size and aspect ratio of the simulated field pattern when these quantities are small as opposed to when they are large. For instance, the difference in the expected proportion of multiclass pixels is much greater between simulated scenes with field aspect ratios of 0.25 and 0.1 than between scenes with field aspect ratios of 1.0 and 0.5. These differences are also greater when the size of the simulated field is 20 acres than when it is 100 acres.

Increasing the size of the simulated fields while holding the aspect ratio fixed decreases the expected proportion of multiclass pixels. Increasing the aspect ratio of the simulated fields while holding their size constant also decreases the expected proportion of multiclass pixels. The proportion of multiclass pixels is decreased significantly by the use of the smaller pixels; for example, a 30x30 m pixel yields less than 1/2 the proportion of 57x79 m pixels and the 10x10 m pixel that might be associated with high-altitude aircraft scanner data yields only 1/6 the proportion. (Obviously, the estimation procedure breaks down for the 57x79 m pixel and the lower, field aspect ratios.) From Fig. 8 the expected proportion of multiclass pixels in the Ellis site is approximately 0.52 for a 57x79 m pixel whereas it is only about 0.23 for a 30x30 m pixel. (The difference in this value for the 57x79 m pixel from that in Table I is due to the approximations used in Eq. (8).)

In Figs. 9 and 10 the expected proportions of multiclass pixels in data containing one-half pixel and one full pixel of misregistration, both along the scan line and perpendicular to it, are plotted together with the same proportion for perfectly registered data, for pixel dimensions of 57x79 m and 30x30 m, respectively. For the 57x79 m pixel $R'(m_w)$ equals 1.28 R for m_w equal to 0.5 and equals 1.43 R for m_w equal to 1.0, that is, misregistration increases the proportion of multiclass pixels by 28% and 43%, respectively. For the same pixel, $R'(m_h)$ equals 1.36 R for m_h equal to 0.5 and equals 1.57 R for m_h equal to 1.0. The difference in the effects of equivalent fractional pixel misregistrations in the two orientations considered is attributable to the unequal height and width of the pixel. For the 30x30 m pixel, $R'(m_h)$ and $R'(m_w)$ are equal whenever m_h and m_w are equal because the pixel is square; $R'(m_h)$ equals 1.32 R for m_h equal to 0.5 and equals 1.5 R for m_h equal to 1.0. The effect of misregistration is equivalent to increasing the dimensions of the pixel by a factor determined by the shape of the pixel and the amount and direction of the misregistration. This effective increase in pixel size results in the increase in the expected proportion of multiclass pixels as illustrated in the two figures.

Fig. 11 is a plot of the multiplicative factor $[1 + p_c(m)]$ by which the expected proportion of multiclass pixels in perfectly registered data is increased due to a fractional pixel misregistration of m, for a pixel whose shape is that of a square. The subscripts used previously on the parameter m have been dropped in this case because the square pixel shape negates the directional effects of the misregistration. The plot is obtained as a function of m by substituting r equals 1 into either Eq. (11) or (12). The plot demonstrates the significant increase in the expected proportion of multiclass pixels even for small amounts of misregistration. The plot also illustrates the nonlinearity of the relationship between this increase and the amount of misregistration.
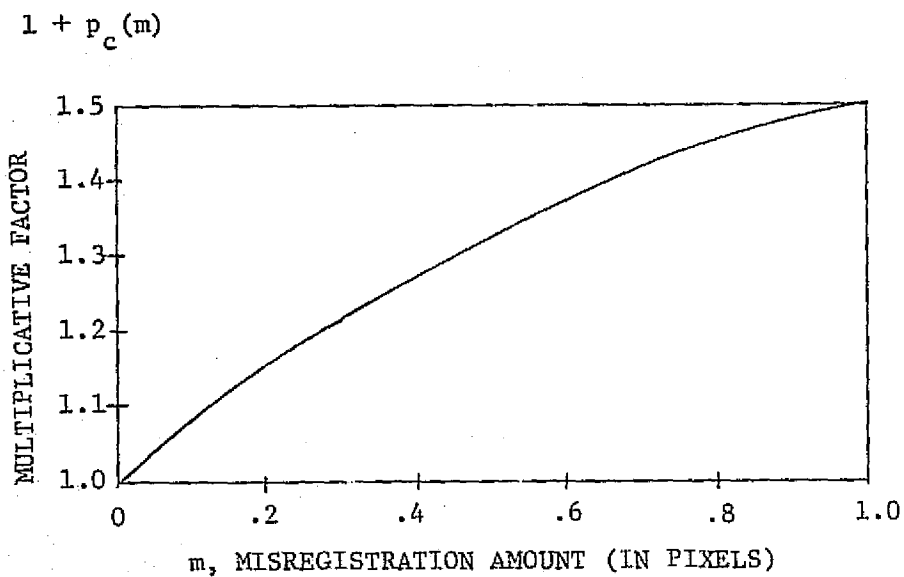
31

$1 + p_c(m)$

FIGURE 11. MULTIPLICATIVE FACTOR DETERMINING INCREASE IN
EXPECTED PROPORTION OF MULTICLASS PIXELS FOR
FRACTIONAL MISREGISTRATION m AND A SQUARE
PIXEL SHAPE

5

THEORETICAL ANALYSIS OF MISREGISTRATION EFFECTS
ON RECOGNITION PERFORMANCE

As noted earlier, spatial misregistration effects for single-class
(field-center) pixels were considered separately from those for multi-
class (e.g., mixture) pixels. Analyses and derivations of simulation
models are presented in Secs. 5.1 and 5.2, with Sec. 5.3 containing an
overall discussion of the effects of misregistration on recognition
performance.

5.1 ANALYSIS FOR SINGLE-CLASS PIXELS

Pixels in this category remain single-class pixels even after mis-
registration. The only effect of misregistration on data and signatures
then is on the correlation between misregistered channels. Horwitz,
et al, [6] and Coberly [7] have analyzed the correlation between the
multispectral signals from ground resolution elements as a function of
ground distance between their centers. Although both studied aircraft
multispectral scanner data, conclusions were drawn for LANDSAT-size
resolution elements. What was found indicates that correlation between
channels drops exponentially as registered pixels move out of registra-
tion. Their results indicate for agricultural data that misregistration
of field-center pixels would reduce the correlation between misregistered
channels and that signals from adjacent LANDSAT pixels would be virtu-
ally uncorrelated. Specific studies of spatial correlation between
LANDSAT pixels were not made during this investigation.

An analytical solution for probability of misclassification as a
function of correlation can be obtained for the special case of two
multivariate normal distributions with a common variance-covariance
matrix. Such a relationship is discussed in Sec. 5.1.1. A signature
simulation model for more general cases is presented in Sec. 5.1.2.

33

5.1.1 ANALYTICAL SOLUTION FOR THE TWO-DISTRIBUTION CASE

When consideration is limited to two multivariate normal dis-
tributions with a common variance-covariance matrix, mathematical
simplifications enable one to derive analytical expressions for the
probability of misclassifying samples from the two distributions.
Derivations of such expressions in terms of between-channel correla-
tion coefficients are presented in App. I and are briefly summarized
here.

First, the optimum quadratic decision rule reduces to a linear
decision rule for two distributions with a common covariance matrix,
which simplifies the analysis. It is shown in App. I that critical
values of correlation exist in the expression for probability of mis-
classification (POM) as a function of the correlation coefficient ρ
between any pair of spectral channels. The maximum probability of
misclassification occurs for:

$$\rho_c = \frac{\mu_1 \sigma_2}{\mu_2 \sigma_1} \quad \text{or} \quad \frac{\mu_2 \sigma_1}{\mu_1 \sigma_2} \qquad \text{for} \quad -1 < \rho < 1$$

where ρ_c is the critical correlation value,

   μ_1 and μ_2 are the differences between means of the
        distributions in Channels 1 and 2,
        respectively,

and σ_1 and σ_2 are the common standard deviations in the
        two channels.

For $\rho_c \neq \pm 1$, the probability of misclassification is zero for
$\rho = \pm 1$, so a plot of probability of misclassification vs. correlation
coefficient might appear as shown in Fig. 12 (other possibilities are
presented and discussed in App. I). Probability of misclassification
is a maximum at $\rho = \rho_c$. The fact the misregistration decreases corre-
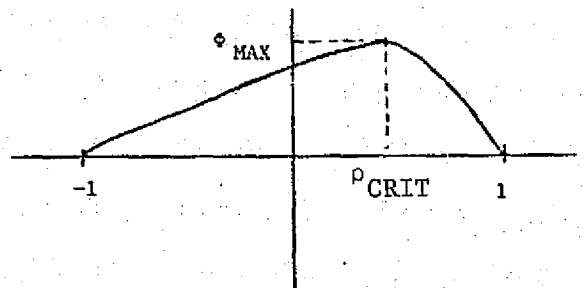lation has already been discussed. Thus, if the actual ρ were between

34

FIGURE 12. ONE ILLUSTRATIVE EXAMPLE OF PROBABILITY
OF MISCLASSIFICATION, ϕ, AS A FUNCTION
OF CORRELATION ρ IN FIELD CENTERS, FOR
TWO NORMAL DISTRIBUTIONS WITH COMMON
COVARIANCE MATRIX.

zero and ρ_c, a misregistration with its consequent decorrelation could actually decrease the probability of misclassification, contrary to usual expectations. Other simulation studies [2,3,8] have shown the net effect of such situations on field-center classification accuracy to be slight, but it is interesting to explor a little further the mechanism by which such decreases would occur.

Fig. 13 presents ellipses representing two distributions with common covariance for three different correlation coefficients. Points along an ellipse are equidistant from the center of the distribution, in a statistical sense. The middle ellipses correspond to the critical correlation value. The line connecting the means passes through these critical ellipses at the point where they are tangent to the super-scribing rectangles. Thus, the statistical distance between the two distributions is shorter (fewest deviation units) for these ellipses than for those of any other correlation value. The "fattest" ellipses correspond to a correlation coefficient of zero. It is clear that if one were to start with $\rho = \rho_c$ and decorrelate, the distance between distributions would increase and probability of misclassification decrease, as illustrated previously. There also would be a re-orientation of the decision boundary between the two distributions.

For the special cases, $\rho_c = \pm 1$, the maximum probability of mis-classification would occur at $\rho = \rho_c$ and the minimum (zero) at $\rho = \mp 1$.

All discussion thus far has been for two channels. App. I shows that the results can be generalized to n channels. Depending on the particular signatures involved, misregistration might tend to increase the probability of misclassification for some channel pairs but decrease it for others. Also, in a multiclass scene, the effects on different pairs of signatures may be different. Simulation is required in order to consider these effects in the analysis due to the mathematical com-plexities required for further analytical efforts.
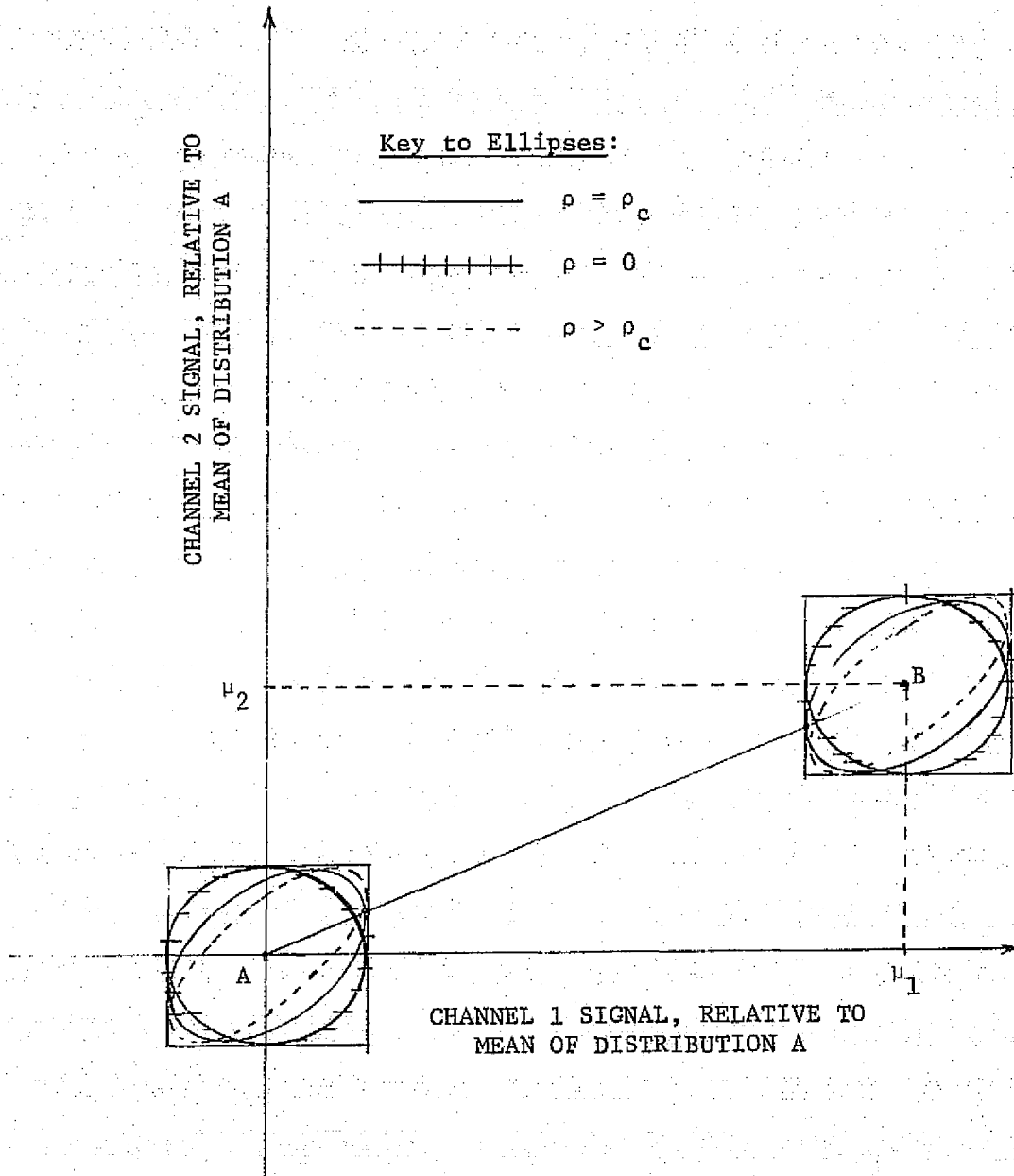
FIGURE 13. ILLUSTRATION OF CRITICAL CORRELATION FOR TWO
DISTRIBUTIONS WITH COMMON COVARIANCE MATRIX

5.1.2 SIMULATION MODEL FOR MISREGISTERED SINGLE-CLASS PIXELS

The model to simulate signatures from misregistered field-center pixels was developed last year [2]. This model assumes that between-channel correlation is a decreasing linear function of misregistration. (See Sec. 5.2 for additional discussion of this assumption.) To be specific, let a perfectly registered distribution S_R have mean A_R and covariance C_R. With some channel or channels misregistered, S_R would have the same mean vector A_R but a different covariance C_M. Any term of C_M, say c_{Mij} would be related to a term of C_R in the following manner:

$$c_{Mij} = c_{Rij} \quad \text{for } i=j$$

$$c_{Mij} = \beta c_{Rij} \quad \text{for } i \neq j, \ 0 \leq \beta \leq 1$$

(21)

where

   β is dependent linearly on the degree of misregistration, i.e., $\beta = 1$ denotes no misregistration, and $\beta = 0$ denotes misregistration by one or more pixels.

Thus, if two channels i and j were misregistered by one-half pixel with respect to one another, then the covariance between i and j, c_{Mij}, would be simulated to be one-half the measured covariance between i and j in the registered signatures.

5.2 ANALYSIS FOR MULTICLASS PIXELS

Pixels considered in this section contain contributions from more than one scene class, either before or after misregistration or both before and after. They usually occur at or near field boundaries as mixture pixels. This section is devoted to describing the development of an improved signature simulation model for which details are presented in App. II. This model was to have been employed in analyses

of signatures extracted from the accurately registered data which were not received. Although the intended analysis could not be carried out, the model was tested and used in analyses of S-192 scanner data under the SKYLAB investigation [3] which jointly supported its development. Sec. 5.2.2 discusses the effects of misregistration on the classification of multiclass pixels.

Consider the case where the signal detected in one or more channels represents a mixture of ground cover W and some other ground cover O. Furthermore, let there be misregistration between the channels. An n-channel multispectral signature for material W consists of a mean vector A_w with components a_{wi} where $i = 1,\ldots,n$, and a covariance matrix C_w with components $c_{wi,j}$ for each $i = 1,\ldots,n$ and $j = 1,\ldots,n$. Similarly, there is a mean vector A_o and covariance matrix C_o for the other ground cover.

To construct the signature of multiclass pixels from the pure signatures of W and O, let α_{wi} be the proportion of cover W present for each pixel in channel i and $\alpha_{oi} = 1 - \alpha_{wi}$ be the corresponding proportion of cover O present for each pixel. If the pixel were of pure cover W then $\alpha_{wi} = 1$ for all i. The mean vector A_M of a mixture distribution of crops W and O can be expressed in each channel i as:

$$A_{Mi} = \alpha_{wi} A_{wi} + (1 - \alpha_{wi}) A_{oi} \tag{22}$$

Any term $c_{Mi,j}$ of the variance-covariance matrix can be expressed as:

$$c_{Mi,j} = \min(\alpha_{wi},\alpha_{wj})\, c_{wi,j} + \min(\alpha_{oi},\alpha_{oj})\, c_{oi,j} \tag{23}$$

Equation (23) describes the estimated covariance between any two channels of data as a function of the amount of misregistration being simulated for multiclass pixels. The coefficients α_{wi} and α_{wj} are equal for the case of no misregistration. A detailed derivation of

this key relationship is presented in App. II, including an extension
to misregistration in two dimensions simultaneously.

Letting $\alpha_{wj} = \alpha_{wi}$ and $\alpha_{oj} = \alpha_{oi}$ in Eq. (23), we have:

$$c_{Mi,j} = \alpha_{wi} \, c_{wi,j} + \alpha_{oi} \, c_{oi,j} \tag{24}$$

which is equivalent to the mixture estimation model previously
developed and implemented at the Environmental Research Institute of
Michigan [9]. A notable feature of both Eqs. (23) and (24) is that
the weighting factors for the covariance terms are in terms of the
first power of the mixture fractions, rather than the second power
which would result if one modeled each mixture pixel as a simple
weighted sum of two random variables.

Let us next consider the covariance terms between channels in
more detail in an attempt to more fully describe and justify the under-
lying assumptions made in the derivation of this simulation model.

Figure 14 displays a possible configuration of the composite
signal received by six different channels (or sets of channels in the
case of multitemporal data) while viewing a single resolution element.
Figure 14(a) indicates that all six channels are viewing precisely the
same location, a borderline resolution element of wheat. This indi-
cates a perfectly registered vector of signals. Figure 14(b) indicates
a vector wherein Channels 3, 5, and 6 are misregistered and actually
viewing mixtures of wheat and other.

Covariances for Channels 1, 2, and 4 would remain identical in
Fig. 14(b) to their values for the case shown in Fig. 14(a). The
covariance for Channels 3 and 5 can be computed with the mixtures
model (Eq. (24)), since they are in registration with each other.
However, in the presence of misregistration, such as between Channels
1 and 3 or 3 and 6, the generalized equation (Eq. (23)) is required for
the covariance computation.

(a) Perfectly Registered   (b) Misregistered
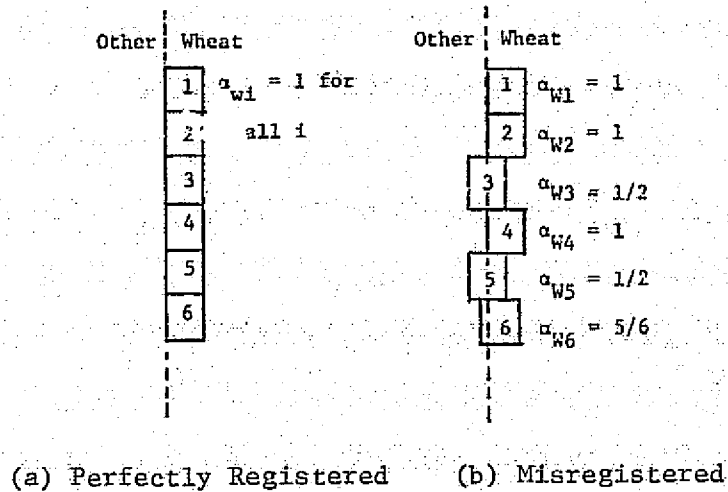
FIGURE 14.   AN EXAMPLE OF CHANNEL MISREGISTRATION
FOR A SINGLE RESOLUTION ELEMENT

(a) Misregistered   (b) Totally Misregistered
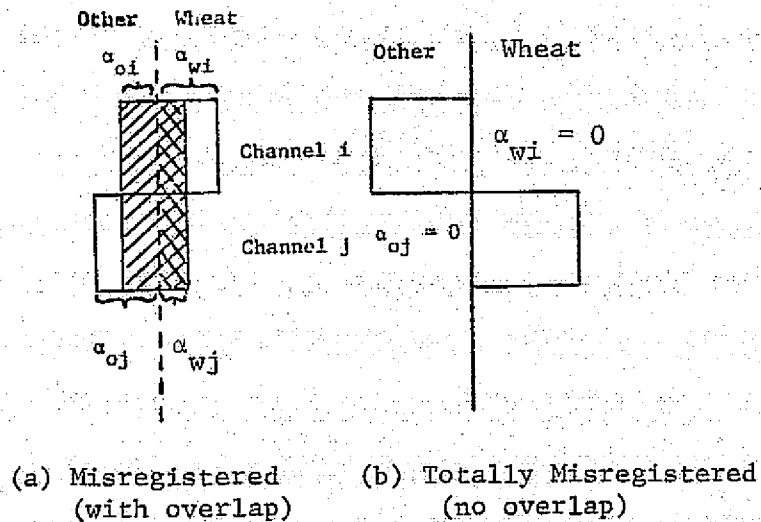(with overlap)   (no overlap)

FIGURE 15.   A MISREGISTRATION CONFIGURATION IN TWO CHANNELS
FOR A SINGLE RESOLUTION ELEMENT, ILLUSTRATING
WEIGHTING FACTORS IN COVARIANCE MODEL

41

Figure 15(a) displays the areas associated with the various com-
ponents of Eq. (23). Note that $\alpha_{wj} = \min(\alpha_{wi}, \alpha_{wj})$ gives the propor-
tion of overlap (area cross-hatched) between the two channels in the
wheat field. Hence $\alpha_{wj} c_{wi,j}$ is the contribution of $c_{wi,j}$ to the con-
structed covariance term $c_{Mi,j}$. Similarly, $\alpha_{oi} = \min(\alpha_{oi}, \alpha_{oj})$ is the
proportion of the other field that is common to both channels i and j
(area hatched) and $\alpha_{oi} c_{oi,j}$ is the contribution of the covariance of
'other' in channels i and j. Hence, where there is no overlap (unshaded
area), the cross correlation is assumed to be negligible and therefore
zero.

Figure 16 illustrates a comparison between the covariance esti-
mated by the derived model and two hypothetical true covariance func-
tions. The differences between the model and the two other curves at
$(1 - \alpha_i) = 1$ could be caused by a finite correlation between adjacent
pixels and/or by scanner noise and atmospheric noise contributions
which were not considered in the model. Studies similar to, and in
addition to, those of Refs. 6 and 7 would be required on satellite
data as well as aircraft data to better define the true functional
relationship.

5.3 DISCUSSION

It was shown in Sec. 4 that a major effect of misregistration
is to reduce the percentage of field-center or single-class pixels
in a scene and correspondingly increase the percentage of multiclass
pixels. Another effect is the reduction of correlation between sig-
nals in misregistered channels. The simulation models developed earlier
in this section allow one to explore the effects of these changes on
recognition performance. We here consider and summarize these effects
in a qualitative manner for LACIE multitemporal recognition, relying
on experience gained in using these models in other work on spectrally
misregistered single-pass S-192 data and multitemporally misregistered
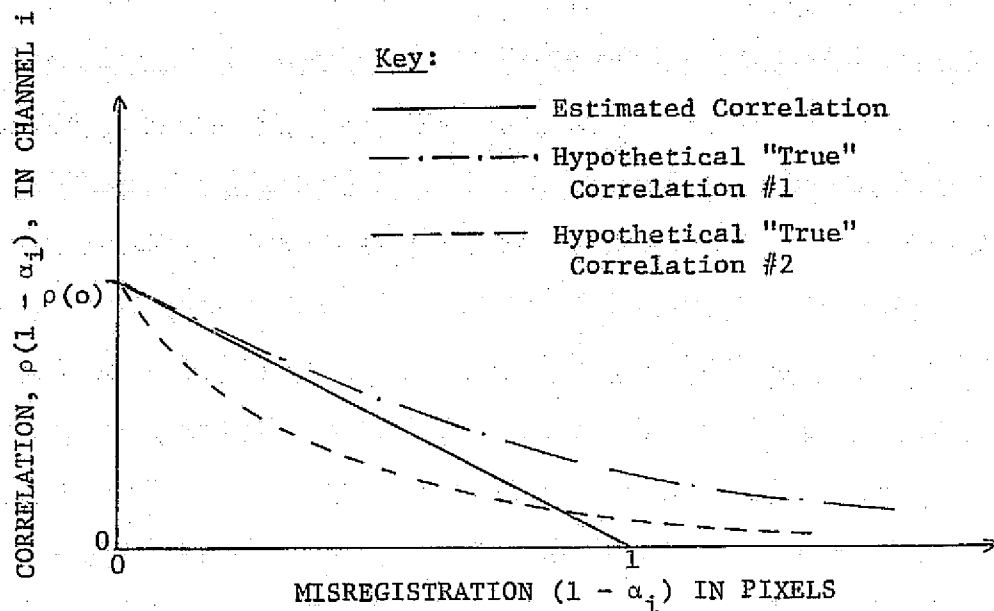two-pass CITARS data.

FIGURE 16. COMPARISON OF THE CORRELATION FUNCTION IN THE SIMULATION
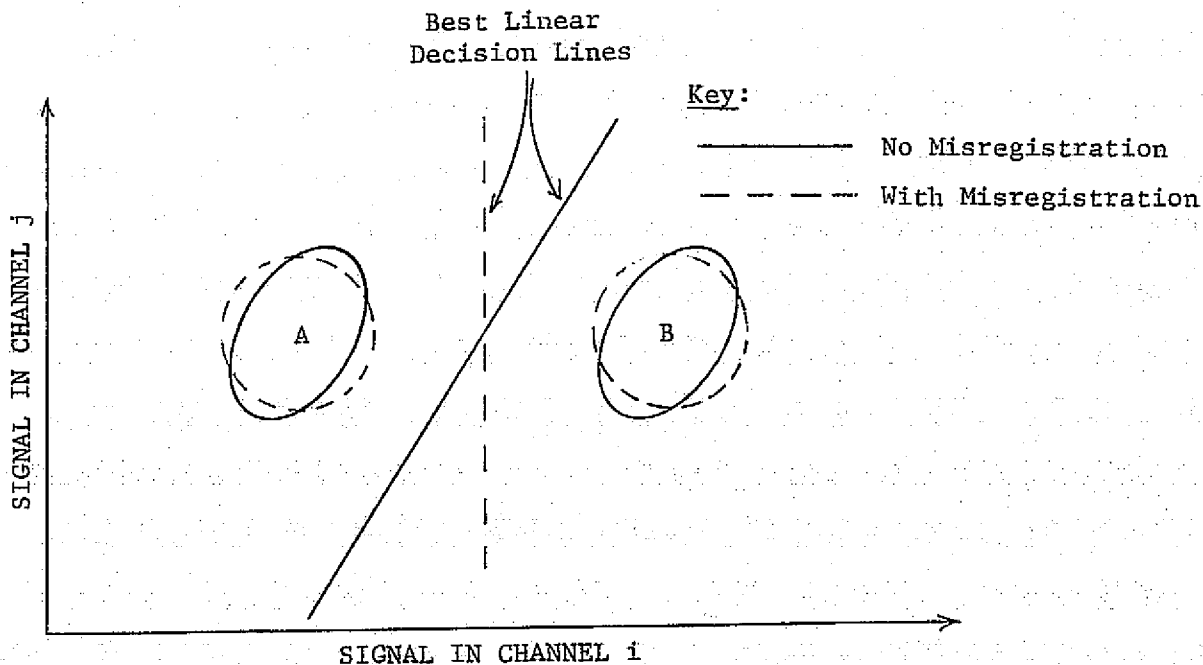MODEL WITH HYPOTHETICAL "TRUE" CORRELATION FUNCTIONS

FIGURE 17. ILLUSTRATION OF MISREGISTRATION EFFECTS
FOR SINGLE-CLASS PIXELS

Fig. 17 illustrates misregistration effects in field centers for single-class pixels. The "fattened" ellipses and the rotated decision line are consequences of misregistration. As discussed in Sec. 5.1.1, probability of misclassification between pairs of classes might increase or decrease upon misregistration, depending on the relative positions, shapes, and orientations of the class ellipses (representing the distributions of signals in the classes). Experience to date has shown these effects to be minor in simulations using multiple channels and multiple classes in agricultural scenes.

The situation is more complex for multiclass pixels, as illustrated in Fig. 18. With no misregistration, multiclass pixels would be simple mixture pixels. The means of their distributions, as seen in Fig. 18(a), would lie along a line, such as $\overline{AB}$, for mixtures of scene classes A and B.

With 1/2-pixel misregistration, the pattern of mixture distributions would split and change, as shown in Fig. 18(b). The rounder ellipses indicate the decorrelation effect within individual classes. The mixture distributions would be shifted symmetrically away from the no-misregistration line of mixture means, causing some of them to be much closer to the competing signature classes, C and D. This shifting would result in greater probabilities of falsely identifying mixtures of A and B as samples of classes C or D. The effect would be intensified even more with a misregistration of one pixel (See Fig. 18(c)).

The above examples and the previously referenced simulation work do indicate that misregistration can adversely affect recognition performance with misregistered data. The errors produced by misregistration will not necessarily compensate either for each other or for recognition errors due to other sources. The effects depend on the particular signature configuration encountered. That is the main reason for the originally planned simulation of registration errors in selected LACIE multitemporal data sets. The use of accurately

44
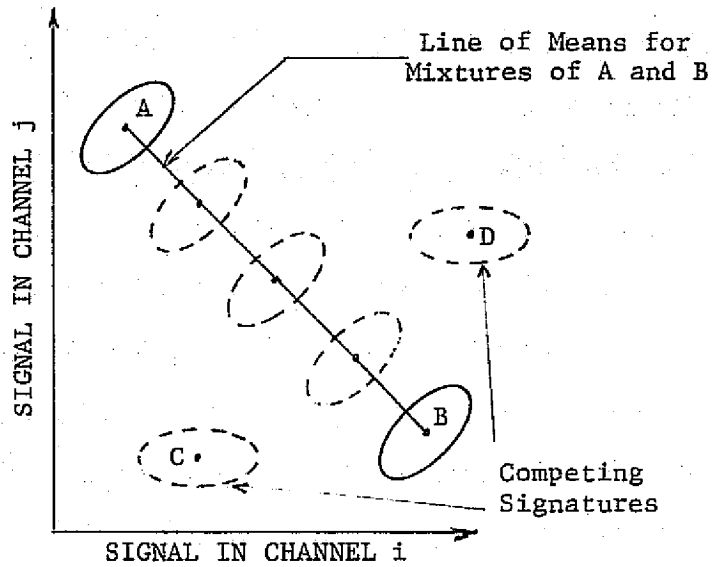
(a) No Misregistration
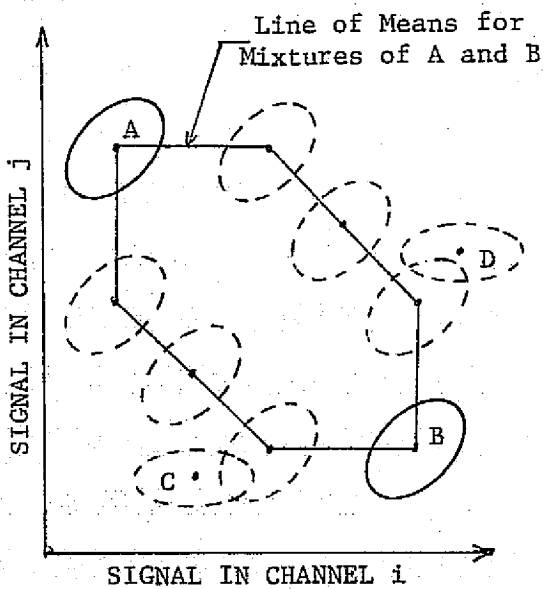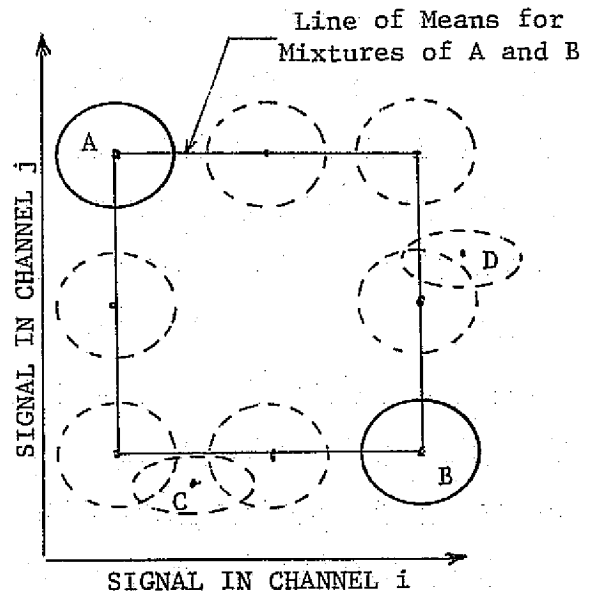
(b) 1/2-Pixel Misregistration   (c) 1-Pixel Misregistration

FIGURE 18.   ILLUSTRATION OF MISREGISTRATION EFFECTS
FOR MULTICLASS PIXELS

registered data for extracting the base single-class signatures was deemed essential because between-time-period correlation was the least known parameter in the prior simulation study. It also would be desirable to develop some analytical measures which are less dependent on particular signature configurations.

6
EMPIRICAL ANALYSIS OF MISREGISTRATION EFFECTS ON RECOGNITION PERFORMANCE

In preparation for the receipt of accurately registered data, computer programs were written to deliberately misregister these data by fixed amounts, either along the scan line or between scan lines. They implemented a cubic convolution algorithm [10] for interpolating data values.

As indicated earlier, the opportunity to apply these programs did not occur. They would have completed a two-step procedure for generating data misregistered by known amounts for analysis purposes. Such data would have served useful ends. However, we note that a more radiometrically accurate procedure that should be considered in future work is a single-step procedure going directly from unregistered scenes to deliberately misregistered data.

A test also was made to determine the amount of between-channel misregistration in single-time Landsat scenes. A procedure developed under another investigation [3] was used for this measurement. The cross-correlation function between signals from pairs of Landsat channels was computed at fractional pixel increments. The amount of misregistration was estimated by the shift parameters corresponding to the peak of the cross-correlation function for ten scan lines, each having 500 points. Both an average misregistration and the standard deviation of that average were computed. Results are presented in Table II for two pairs of channels, (1,2) and (3,4). The signals for the other combinations of channel pairs were not highly enough correlated to yield meaningful results. The results in Table II indicate that no significant amount of misregistration is present between the given channels in these single-time Landsat data sets. Although precise results were not obtained for the remaining channel pairs, there has been no evidence of which we are aware to indicate that a significant amount of misregistration exists between any pairs of the four Landsat channels.

FORMERLY WILLOW RUN LABORATORIES, THE UNIVERSITY OF MICHIGAN

TABLE II. ACCURACY OF BETWEEN-CHANNEL REGISTRATION
IN LANDSAT MSS DATA

Data Segment:	Finney, Kansas 26 May 74		Ellis, Kansas 12 June 74	
Channel Pair	Average Misregistration (Pixels)	Standard Deviation of the Average	Average Misregistration (Pixels)	Standard Deviation of the Average
1-2	-0.068	0.026	-0.035	0.014
3-4	-0.089	0.013	-0.055	0.014

APPENDIX I

A SIMPLE ANALYTICAL MODEL TO STUDY THE EFFECTS OF MISREGISTRATION ON FIELD CENTER CLASSIFICATION ACCURACY

Insight has been gained into what effects spatial misregistration may have on field-center classification accuracy through an analytical analysis of the problem. Consider two normal distributions in n channels, $N_A(\mu_A, R)$ and $N_B(\mu_B, R)$, with a common covariance R. The probability of a type-one error[*] using the best linear decision rule is

$$\Phi[1/2(\mu^t R^{-1} \mu)^{\frac{1}{2}}] \tag{I-1}$$

where

$$\Phi(x) = \frac{1}{\sqrt{2\pi}} \int_x^\infty e^{-\frac{1}{2} y^2} dy \tag{I-2}$$

and $\mu = \mu_A - \mu_B$, the channel to channel mean difference.

Studies have indicated that misregistration from channel to channel, or time period to time period in the case of multitemporal analyses, causes resultant signatures to be less correlated. This analysis, therefore, attempts to examine the error rate Φ as a function of correlation ρ.

$$\text{Let } R = \begin{pmatrix} \sigma_1^2 & \rho\sigma_1\sigma_2 \\ \rho\sigma_1\sigma_2 & \sigma_2^2 \end{pmatrix} \quad ; \quad \text{then } R^{-1} = \frac{1}{\sigma_1^2\sigma_2^2(1-\rho^2)} \begin{pmatrix} \sigma_2^2 & -\rho\sigma_1\sigma_2 \\ -\rho\sigma_1\sigma_2 & \sigma_1^2 \end{pmatrix} \tag{I-3}$$

---

[*]Under the assumption of common covariance, type-two error is equivalent to type-one error.

Also, let $f(\rho) = \mu^t R^{-1} \mu$ for $-1 \le \rho \le 1$ (I-4)

and $g(\rho) = 1/2 f(\rho)^{1/2}$

       $f(\rho) \to \infty$ at $\rho = \pm 1$, except for $\mu_2 = \pm \mu_1 \left(\dfrac{\sigma_1}{\sigma_2} \right)$

Similarly $g(\rho) \to \infty$ at $\rho = \pm 1$, which implies $x \to \infty$ at $\rho = \pm 1$. Φ can be expressed as a function of ρ through $f(\rho)$ and/or $g(\rho)$:

       $\Phi(x) = \Phi[1/2 \ f(\rho)^{1/2}] = \Phi[g(\rho)].$

Substituting $x = \infty$ into Eq. I-2 we have $I(\infty) = 0$. We have established therefore, that the error rate Φ is minimized for correlation $\rho = \pm 1$. The only exceptions are when $\mu_2 = \mu_1 \ (\sigma_1/\sigma_2)$ for $\rho = +1$ and when $\mu_2 = -\mu_1 \ (\sigma_1/\sigma_2)$ for $\rho = -1$, in which cases Φ has a finite value which will be shown later to be a maximum of $\Phi(g(\rho))$. Let us now examine the behavior of the function Φ for $-1 < \rho < 1$.

Although restricting ourselves to two channels we note that the following analysis can be generalized for ρ_{ij}, the correlation between any pair of channels i and j.

Let us now calculate the first derivative of $f(\rho)$:

       $f(\rho) = \mu^t R^{-1} \mu$

       $\dfrac{df(\rho)}{d(\rho)} = \mu^t \ \dfrac{d \ R^{-1}}{d\rho} \ \mu$ (I-5)

We can simplify the calculation of $\dfrac{d\,R^{-1}}{d\rho}$ by noting the following relationship between $\dfrac{dR^{-1}}{d\rho}$ and $\dfrac{dR}{d\rho}$:

$$\frac{d}{d\rho}\,(RR^{-1}) = \frac{d}{d\rho}\,(I) = 0 = \left(\frac{dR}{d\rho}\right)R^{-1} + R\left(\frac{dR^{-1}}{d\rho}\right)$$

Solving for $\dfrac{dR^{-1}}{d\rho}$ we find:

$$\frac{dR^{-1}}{d\rho} = -R^{-1}\left(\frac{dR}{d\rho}\right)R^{-1} \tag{I-6}$$

Substituting Eq. I-6 into Eq. I-5 and solving:

$$\frac{df(\rho)}{d\rho} = -\mu^t R^{-1}\,\frac{dR}{d\rho}\,R^{-1}\mu$$

Noting that $\mu^t R^{-1} = [(R^{-1})^t \mu]^t$ and $(R^{-1})^t = R^{-1}$

$$\frac{df(\rho)}{d\rho} = -(R^{-1}\mu)^t\,\frac{dR}{d\rho}\,(R^{-1}\mu) \tag{I-7}$$

Eq. I-7 is an expression for the first derivative of $f(\rho)$ in terms of the derivative of R. Now let us examine if, for $-1 < \rho < 1$, critical values of $f(\rho)$ exist. Individually examining the components of Equation (I-6), we determine the following expression for two channels:

$$R^{-1}\mu = \frac{1}{\sigma_1^2 \sigma_1^2\,(1-\rho^2)}\begin{pmatrix} \sigma_2^2\mu_1 - \rho\sigma_1\sigma_2\mu_2 \\ \sigma_1^2\mu_2 - \rho\sigma_1\sigma_2\mu_1 \end{pmatrix} \equiv c_1 \begin{pmatrix} a_1 \\ a_2 \end{pmatrix} \tag{I-8}$$

$$\frac{dR}{d\rho} = \sigma_1\sigma_2 \begin{pmatrix} 0 & 1 \\ 1 & 0 \end{pmatrix} = c_2 \begin{pmatrix} 0 & 1 \\ 1 & 0 \end{pmatrix} \tag{I-9}$$

Now substituting I-8 and I-9 into I-7:

$$\frac{df(\rho)}{d\rho} = -c_1(a_1, \; a_2) \; c_2 \begin{pmatrix} 0 & 1 \\ 1 & 0 \end{pmatrix} c_1 \begin{pmatrix} a_1 \\ a_2 \end{pmatrix}; \quad \text{let } b = -c_2 c_1^{\,2} \qquad \text{(I-10)}$$

$$\frac{df(\rho)}{d\rho} = b(a_1 a_2) \begin{pmatrix} a_2 \\ a_1 \end{pmatrix} = 2b a_1 a_2 ; \; b > 0 \qquad \text{(I-11)}$$

For $\dfrac{df(\rho)}{d\rho} = 0$, either a_1 or a_2, one of the two rows of R^{-1}, must equal zero. Since $\Phi(x) \geq 0$ and continuous, and has minima (zeroes) defined at $\rho = \pm 1$, then Φ is maximized at

$$\rho_C = \frac{\mu_1 \sigma_2}{\mu_2 \sigma_1} \quad \text{or} \quad \frac{\mu_2 \sigma_1}{\mu_1 \sigma_2} \; \text{ for } -1 < \rho < 1. \qquad \text{(I-12)}$$

For the special cases when $\mu_2 = + \mu_1 \left(\dfrac{\sigma_1}{\sigma_2} \right)$ and $\mu_2 = - \mu_2 \left(\dfrac{\sigma_1}{\sigma_2} \right)$, Φ continues to have a minimum at $\rho = -1$ and $\rho = +1$, respectively. However, at $\rho = +1$ and -1 for these cases, respectively, Eq. (I-12) applies and shows that Φ has a maximum.

Before examining the implications of this result, let us show how this result can be generalized.

Eqs. I-5 to I-7 can be generalized by letting $\rho = \rho_{ij}$ and $\dfrac{dR}{d\rho} = \dfrac{\partial R}{\partial \rho_{ij}}$ for any pair of channels i and j.

Hence:

$$f(\rho_{ij}) = \mu^t R^{-1} \mu$$

and

$$\frac{\partial f(\rho_{ij})}{\partial \rho} = \mu^t \frac{\partial R^{-1}}{\partial \rho_{ij}} \mu$$

Examining a three-dimensional case,

$$R = \begin{pmatrix} \sigma_1^2 & \rho_{12}\sigma_1\sigma_2 & \rho_{13}\sigma_1\sigma_3 \\ \rho_{12}\sigma_1\sigma_2 & \sigma_2^2 & \rho_{23}\sigma_2\sigma_? \\ \rho_{13}\sigma_1\sigma_3 & \rho_{23}\sigma_2\sigma_3 & \sigma_3^2 \end{pmatrix}$$

Therefore:

$$\frac{\partial R}{\partial \rho_{12}} = \begin{pmatrix} 0 & 1 & 0 \\ 1 & 0 & 0 \\ 0 & 0 & 0 \end{pmatrix} \; ; \quad \frac{\partial R}{\partial \rho_{13}} = \begin{pmatrix} 0 & 0 & 1 \\ 0 & 0 & 0 \\ 1 & 0 & 0 \end{pmatrix} \; ; \quad \frac{\partial R}{\partial \rho_{23}} = \begin{pmatrix} 0 & 0 & 0 \\ 0 & 0 & 1 \\ 0 & 1 & 0 \end{pmatrix}$$

Following the same line of reasoning as in two dimensions [Eq. I-10 and I-11] we find that

$$\frac{\partial f(\rho_{12})}{\partial \rho_{12}} = 0 \text{ when either the 1st or 2nd row of } R^{-1}\mu \text{ is zero;}$$

similarly for $f(\rho_{23})$ and $f(\rho_{13})$.

We can now generalize to conclude

$$\frac{\partial f(\rho_{i,j})}{\partial \rho_{i,j}} = 0 \text{ at some } \rho_{ci,j} \text{ in the interval defined by } -1 < \rho_{ij} < 1$$

for any pair of channels i, j. The point $\rho_{ci,j}$ can be calculated exactly by setting the ith or j^{th} row of $R^{-1}\mu$ equal to zero and solving for $\rho_{i,j}$. The function f is a function of many variables, $f(\rho_{12},\rho_{13},\ldots,\rho_{ij},\ldots)$ for all i,j. We have determined that (1) the function Φ is minimized along its boundary in the interval $-1 \le \rho \le 1$ and (2) the function f has a critical point at $\rho_{ci,j}$ with respect to each variable $\rho_{i,j}$ for all i and j and these critical points must be maxima. Under these conditions we can conclude that the function Φ reaches a maximum on the interval $-1 < \rho_{ij} < 1$.

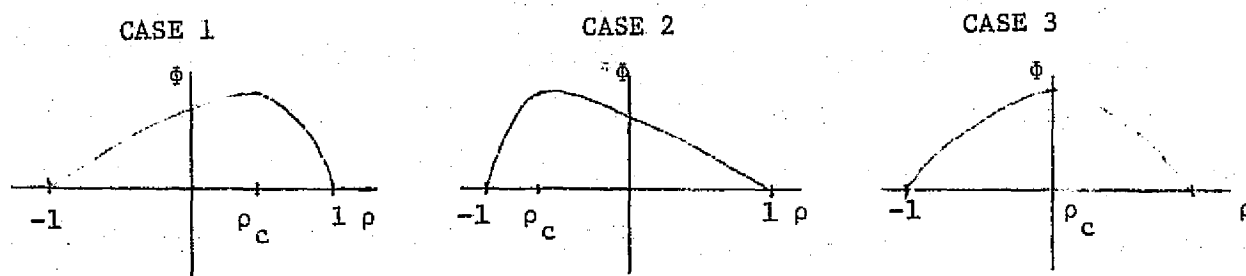Let us now examine the implications of this analysis graphically for two channels of data:

CASE 1   CASE 2   CASE 3

FIGURE I-1. ERROR RATE OF RECOGNITION Φ, AS A FUNCTION
OF CORRELATION ρ IN FIELD CENTERS

Figure I-1 displays possible curves mapping the error rate Φ in field centers as a function of ρ, excluding the special cases with $\rho_c = \pm 1$. A maximum error occurs at ρ_c. Φ is minimized at $\rho = \pm 1$ and intercepts the y axis at $\rho = 0$, $f(0) = f(0) = \dfrac{\mu_1^2 \sigma_2^2 + \mu_2^2 \sigma_1^2}{\sigma_1^2 \sigma_2^2}$.

ρ_c occurs at $\rho_c = \dfrac{\mu_1 \sigma_2}{\mu_2 \sigma_1}$ or $\dfrac{\mu_2 \sigma_1}{\mu_1 \sigma_2}$.

Let ρ_r be the correlation of a registered data set in two channels and let ρ_m be the correlation of the same data set but misregistered to varying degrees. Keep in mind that misregistrating data will cause the correlation to decrease. Let us examine each case depicted in Figure I-1 separately.

CASE 1

(1) If $0 \leq \rho_c \leq \rho_r \leq 1$, then misregistering the data set would cause the error rate to increase until $\rho_m = \rho_c$, then it would restore accuracy somewhat until $\rho_m = 0$.

(2) If $0 \leq \rho_r \leq \rho_c \leq 1$, then misregistration would actually improve results.

(3) If $-1 \leq \rho_r \leq 0$, then misregistration would cause the error rate to increase.

(4) If $\rho_c \approx 1$, misregistration would always improve field center results.

CASE 2

(1) If $-1 \leq \rho_r \leq \rho_c < 0$, this behaves as case 1, step (1).

(2) If $-1 \leq \rho_c \leq \rho_r \leq 0$, see case 1, step (2).

(3) If $0 \leq \rho_r \leq 1$, see case 1, step (3).

(4) If $\rho_c \approx -1$, see case 1, step (4).

CASE 3

In this case misregistration would always cause the error rate to increase.

APPENDIX II

DERIVATION OF COVARIANCE ESTIMATION MODEL FOR
MISREGISTERED MULTICLASS PIXELS

In the derivation of the covariance estimation model, we restrict
ourselves to two channels of data and two crop types. Figure II-1
illustrates a possible configuration of boundary elements for two
channels misregistered with respect to one another. It is the cross-
correlation between two such channels that we are interested in calcu-
lating.
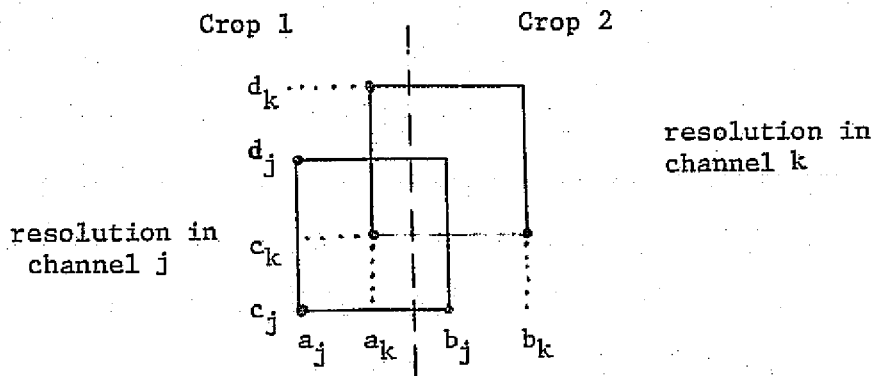
FIGURE II-1. CONFIGURATION OF BOUNDARY RESOLUTION
ELEMENTS OF TWO CHANNELS OF DATA MIS-
REGISTERED WITH RESPECT TO ONE ANOTHER

Let $S_{ij}(\alpha,\beta)$ be the signal per unit area from ground coordinate
(α,β) for the ith crop, j^{th} channel. This signal is assumed to origi-
nate from a stationary random process, with statistics:

$$E[S_{ij}(\alpha,\beta)] = A_{ij}$$

$$E\{[S_{ij}(\alpha_1,\beta_1) - A_{ij}] \ [S_{hk}(\alpha_2,\beta_2) - A_{hk}]\}$$

$$= \delta(i,h) \ r_{ijk} \ (\alpha_1 - \alpha_2, \beta_1 - \beta_2)$$

$\delta(i,h)$ is Kronicker's Delta Function. If $i \neq h$, i.e., two different crops, correlation is assumed to be zero.

$r_{ijk}(\alpha_1 - \alpha_2, \beta_1 - \beta_2)$ is the cross-correlation function and is dependent on the distance between the locations on the ground.

The assumption made is that the correlation between two pixels drops rapidly as the distance between two pixels increases. The correlation between two adjacent pixels is assumed to be zero.

The scanner signal in the jth channel is the sum over the resolution area of all signals $S_{ij}(\alpha,\beta)$:

$$x_j = \int_{a_j}^{0} d\alpha \int_{c_j}^{d_j} d\beta S_{1j}(\alpha,\beta) + \int_{0}^{b_j} d\alpha \int_{c_j}^{d_j} d\beta\, S_{2j}(\alpha,\beta)$$

with statistics:

$$E(x_j) = \int_{a_j}^{0} d\alpha \int_{c_j}^{d_j} d\beta a_{1j} + \int_{0}^{b_j} d\alpha \int_{c_j}^{d_j} d\beta a_{2j}$$

$$x_j - E(x_j) = \int_{a_j}^{0} d\alpha \int_{c_j}^{d_j} d\beta [S_{1j}(\alpha,\beta) - A_{1j}] + \int_{0}^{b_j} d\alpha \int_{c_j}^{d_j} d\beta [S_{2j}(\alpha,\beta) - A_{2j}]$$

The correlation between channels j and k is:

$$R_{jk} = E\left\{[x_j - E(x_j)]\,[x_k - E(x_k)]\right\}$$

$$= E\left\{\left[\int_{a_j}^{0} d\alpha_1 \int_{c_j}^{d_j} d\beta_1 [S_{1j}(\alpha_1,\beta_1) - A_{1j}] + \int_{0}^{b_j} d\alpha_2 \int_{c_j}^{d_j} d\beta_2 [S_{2j}(\alpha_2,\beta_2) - A_{2j}]\right]\right.$$

$$\left. * \left[\int_{a_k}^{0} d\alpha_1 \int_{c_k}^{d_k} d\beta_1 [S_{1k}(\alpha_1,\beta_1) - A_{1k}] + \int_{0}^{b_k} d\alpha_2 \int_{c_k}^{d_k} d\beta [S_{2k}(\alpha_2,\beta_2) - A_{2k}]\right]\right\}$$

Multiplying this expression out we note that cross terms drop out due to Kronecker's Delta:

$$R_{jk} \int_{a_j}^{0} d\alpha_1 \int_{c_j}^{d_j} d\beta_1 \int_{a_k}^{0} d\alpha_2 \int_{c_k}^{d_k} d\beta_2\ r_{1jk}(\alpha_1 - \alpha_2,\ \beta_1 - \beta_2)$$

$$+ \int_{0}^{b_j} d\alpha_1 \int_{c_j}^{d_j} d\beta_1 \int_{0}^{b_k} d\alpha_2 \int_{c_k}^{d_k} d\beta_2\ r_{2jk}(\alpha_1 - \alpha_2,\ \beta_1 - \beta_2)$$

To simplify the algebra let $c_j = c_k$ and $d_j = d_k$. This means that only mis-registration in one direction is considered. We will generalize later to two directions. Using this assumption along with an identity[*],

---

* Simplified using the identity

$$\int_{A}^{B} \int_{A}^{B} F(u-v)\ du\ dv = (B-A) \int_{-(B-A)}^{B-A} F(x) \left(1 - \frac{|x|}{B-A}\right) dx$$

$$R_{jk} = \int_{a_j}^{0} d\alpha_1 \int_{a_k}^{0} d\alpha_2 (d-c) \int_{-(d-c)}^{d-c} r_{1jk}(\alpha_1-\alpha_2,\beta) \left(1 - \frac{|\beta|}{d-c}\right) d\beta$$

$$+ \int_{0}^{b_j} d\alpha_1 \int_{0}^{b_k} d\alpha_2 (d-c) \int_{-(d-c)}^{d-c} r_{2jk}(\alpha_1-\alpha_2,\beta) \left(1 - \frac{|\beta|}{d-c}\right) d\beta$$

Let $\quad F_{1jk} = (d-c) \int_{-(d-c)}^{d-c} r_{1jk}(\alpha_1-\alpha_2,\beta) \left(\frac{1-|\beta|}{d-c}\right) d\beta$

and similarly

$$F_{2jk} = (d-c) \int_{-(d-c)}^{d-c} r_{2jk}(\alpha_1-\alpha_2,\beta) \left(\frac{1-|\beta|}{d-c}\right) d\beta$$

Substituting we have:

$$R_{jk} = \int_{a_j}^{0} d\alpha_1 \int_{a_k}^{0} d\alpha_2 \, F_{1jk}(\alpha_1-\alpha_2) + \int_{0}^{b_j} d\alpha_1 \int_{0}^{b_k} d\alpha_2 F_{2jk}(\alpha_1-\alpha_2) \qquad (II-1)$$

Now examine each component of R_{jk} assuming that $a_j \le a_k$ (the same argument applies otherwise).

$$\int_{a_j}^{0} d\alpha_1 \int_{a_k}^{0} d\alpha_2 \, F_{1jk}(\alpha_1-\alpha_2)$$

$$= \int_{a_j}^{a_k} d\alpha_1 \int_{a_k}^{0} d\alpha_2 \, F_{1jk}(\alpha_2-\alpha_1) + \int_{a_k}^{0} d\alpha_1 \int_{a_k}^{0} d\alpha_2 \, F_{1jk}(\alpha_2-\alpha_1)$$

$$= \int_{a_j}^{a_k} d\alpha_1 \int_{a_k}^{0} d\alpha_2 \, F_{1jk}(\alpha_2-\alpha_1) + (-a_k) \int_{a_k}^{-a_k} F_{1jk}(\alpha) \left(1-\frac{|\alpha|}{-a_k}\right) d\alpha \qquad (II-2)$$

59

The contribution to the estimated covariance from any non-overlapping region is assumed to be zero. The left component of Eq. II-2 determines this contribution, hence it can be eliminated. Thus the left hand term of R_{jk} is:

$$\approx (-a_k) \int_{a_k}^{-a_k} F_{1jk}(\alpha) \left(1-\frac{|\alpha|}{-a_k}\right) \, d\alpha \qquad \text{(II-3)}$$

Similarly for $b_j < b_k$ we find:

$$\int_0^{b_j} d\alpha_1 \int_0^{b_k} d\alpha_2 \, F_{2jk} (\alpha_1-\alpha_2) \approx (b_j) \int_{-b_j}^{b_j} F_{2jk} \left(1-\frac{|\alpha|}{b_j}\right) \, d\alpha \qquad \text{(II-4)}$$

Substituting Eqs. II-3 and II-4 into Eq. II-1 we have:

$$R_{jk} \approx (-a_k) \int_{a_k}^{-a_k} F_{1jk}(\alpha) \left(1-\frac{|\beta|}{-a_k}\right) \, d\alpha + (b_j) \int F_{2jk} \left(1-\frac{|\alpha|}{b_j}\right) \, d\alpha \qquad \text{(II-5)}$$

If the pixels being examined were pure crop 2 pixels, the expression evaluated for R_{jk} would be the covariance R_{2jk} between channels j and k in crop 2. In order to simplify the expression for a border pixel we need to evaluate it in the field center case.

For crop 2, $a_k = 0$ and let $b_j = b_k = b$, hence

$$R_{jk} = R_{2jk} = 0 + \int_0^b d\alpha_1 \int_0^b d\alpha_2 \, F_{2jk} (\alpha_1-\alpha_2)$$

Simplifying:

$$R_{2jk} = b \int_{-b}^b F_{2jk} (\alpha) \left(1-\frac{|\alpha|}{b}\right) \, d\alpha \qquad \text{(II-6)}$$

Similarly for crop 1, $b_j = 0$, and let $a_j = a_k = a$

$$R_{1jk} = a \int_{-a}^{a} F_{1jk} (\alpha) \left(1 - \frac{|\alpha|}{a}\right) d\alpha \tag{II-7}$$

We know have R_{2jk} and R_{1jk}, the covariance terms for channels j and k for crops two and one.

For a mixed pixel, we make two observations.

(1) The covariance of two points on the ground drops very rapidly as a function of the distance between them then:

(2) To substitute Eqs. (II-6) and (II-7) into Eq. (II-5) we need to normalize by dividing respective terms by a and b, the widths of the respective pixels.

Having made these observations we can conclude for a boundary pixel, the covariance R_{jk} can be calculated using the expression

$$R_{jk} = \frac{a_k}{a} R_{1jk} + \frac{b_j}{b} R_{2jk} \tag{II-8}$$

Eq. II-8 was derived under the assumption that misregistration was in only one direction. The simulation model described in Sec. 5.2 is based on this assumption. The analogy of Eq. II-8 with misregistration in two directions is a trivial extension of Eq. II-8 and is determined to be:

$$R_{jk} = \left(\frac{d_k - c_j}{ac}\right) a_k R_{1jk} + \left(\frac{d_k - c_j}{bd}\right) b_j R_{2jk} \tag{II-9}$$

where $c = d_k - c_k$ and $d = d_j - c_j$ are the heights of each resolution element.

We note that in our case the widths of the respective pixels are the same size, hence $a = b$. Therefore, a_k/a is the proportion of overlap in crop 1, and b_j/b is the proportion of overlap in crop 2.

APPENDIX III

DERIVATION OF EXTENSION TO ERIM METHOD TO ACCOUNT FOR EFFECTS OF MISREGISTRATION ON EXPECTED PROPORTION OF MULTICLASS PIXELS

The ERIM method for estimating the expected proportion of multi-class pixels existing in perfectly registered data will be extended to estimate the expected proportion of multiclass pixels in misregistered multitemporal data. In Section 4.2, the situation is discussed in detail and the basic approach to the extension is presented. For misregistration along the scan line of distance Δw, the expected proportion of multiclass pixels is given by

$$R'(\Delta w) = R[1 + p_c(\Delta w)]$$

where R is the expected proportion of multiclass pixels when no mis-registration is present. Similarly, for misregistration between scan lines of distance Δh, the expected proportion of multiclass pixels is given by

$$R'(\Delta h) = [1 + p_c(\Delta h)]$$

The quantities Δh and Δw are restricted to values less than the pixel dimensions h and w, respectively.

Recall that the assumption was made that the boundary segment within each boundary pixel may be considered as a straight line segment. The quantity $p_c(\Delta w)$ which must be determined, is defined as the proba-bility that such a straight line boundary segment, randomly oriented about a point (x,y) within a boundary pixel, will intersect either the top or bottom edge of the pixel within a distance Δw from its left edge. Referring to Fig. 6, the angle α_L between the boundary segment line and the vertical line drawn through the point (x,y) will be assumed to have a uniform probability density $p(\alpha_L)$ over an angle of π radians to the left of the vertical, that is

$$p(\alpha_L) = \frac{1}{\pi} \qquad 0 \le \alpha_L \le \pi$$

The point (x,y) about which the boundary segment is oriented will be assumed to be uniformly distributed within the pixel with probability density p(x) for the x-coordinate, given by

$$p(x) = \frac{1}{w} \qquad 0 < x \le w$$

and probability density p(y) for the y-coordinate, given by

$$p(y) = \frac{1}{h} \qquad 0 < y \le h$$

The angles $\alpha_T(x,y)$ and $\alpha_B(x,y)$ represent the range of angles through which the boundary segment oriented about (x,y) will intersect the two critical areas along the pixel edge. The probability $p_c(\Delta w)$ can then be expressed in terms of these angles, as

$$p_c(\Delta w) = \int_{-\infty}^{\infty} \int_{-\infty}^{\infty} \int_{-\infty}^{\infty} [\alpha_B(x,y) + \alpha_T(x,y)] \, p(x)p(y)p(\alpha_L) \, dy \, dx \, d\alpha_L$$

$$= \frac{1}{\pi hw} \int_{0}^{h} \int_{0}^{w} [\alpha_B(x,y) + \alpha_T(x,y)] \, dx \, dy$$

which due to symmetry can be simplified as

$$p_c(\Delta w) = \frac{2}{\pi hw} \int_{0}^{h} \int_{0}^{w} \alpha_B(x,y) \, dx \, dy$$

The angle $\alpha_B(x,y)$ will now have to be considered as two angles $\alpha_{B1}(x,y)$ and $\alpha_{B2}(x,y)$ depending on whether x is less than or equal to Δw or greater than Δw. Fig. III-1 illustrates each of these angles. In terms of these two angles, $p_c(\Delta w)$ will now be expressed as
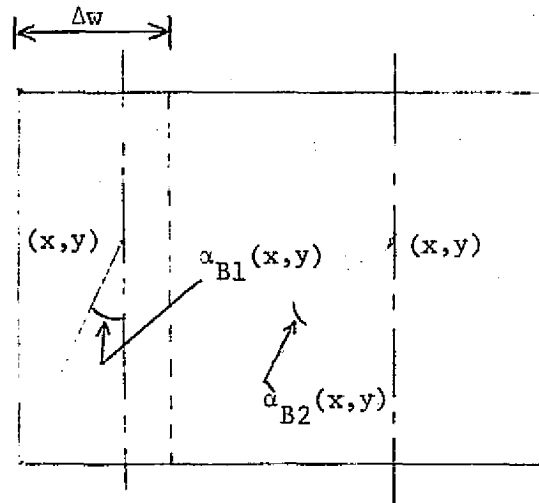
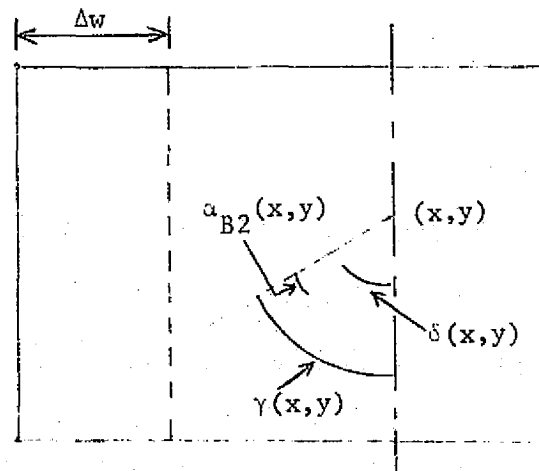FIGURE III-1. ILLUSTRATION OF ANGLES $\alpha_{B1}(x,y)$ AND $\alpha_{B2}(x,y)$

FIGURE III-2. DETERMINATION OF ANGLE $\alpha_{B2}(x,y)$

$$P_c(\Delta w) = \frac{2}{\pi hw} \left[\int_0^h \int_0^{\Delta w} \alpha_{B1}(x,y) \ dx \ dy + \int_0^h \int_{\Delta w}^w \alpha_{B2}(x,y) \ dx \ dy \right]$$

(III-1)

Over the range of x values less than or equal to Δw, $\alpha_{B1}(x,y)$ is equal to

$$\alpha_{B1}(x,y) = \tan^{-1}\left(\frac{x}{y}\right)$$

and the first term in the brackets in Eq. (III-1), denoted as T_1, can then be written as

$$T_1 = \int_0^h \int_0^{\Delta w} \tan^{-1}\left(\frac{x}{y}\right) dx \ dy$$

(III-2)

Using the identity

$$\int \tan^{-1}\left(\frac{u}{a}\right) du = u \ \tan^{-1}\left(\frac{u}{a}\right) - \frac{a}{2} \ln \ (u^2 + a^2)$$

the integration over the variable x in Eq. (III-2) can be performed and evaluated at the proper limits with the result that

$$T_1 = \int_0^h \left[\Delta w \ \cot^{-1}\left(\frac{y}{\Delta w}\right) - \left(\frac{y}{2}\right) \ln \ (y^2 + (\Delta w)^2) \right.$$

$$\left. + \left(\frac{y}{2}\right) \ln(y^2) \right] dy$$

(III-3)

Using the identities

$$\int \cot^{-1}\left(\frac{u}{a}\right) du = u \ \cot^{-1}\left(\frac{u}{a}\right) + \frac{a}{2} \ln \ (u^2 + a^2)$$

$$\int u \ln (u^2 + a^2) \, du = \frac{u^2}{2} \ln(u^2 + a^2) - \int \frac{u^3}{u^2 + a^2} \, du$$

and

$$\int \frac{u^3}{u^2 + a^2} \, du = \frac{u^2}{2} - \frac{a^2}{2} \ln(u^2 + a^2)$$

Eq. (III-3) can be evaluated over the range of integration, with the result

$$T_1 = \frac{(\Delta w)^2}{2} \ln\left(1 + \frac{h^2}{(\Delta w)^2}\right) - \frac{h^2}{2} \ln\left(1 + \frac{(\Delta w)^2}{h^2}\right) + 2\Delta wh \, \cot^{-1}\left(\frac{h}{\Delta w}\right)$$

In Fig. III-2, two angles $\delta(x,y)$ and $\gamma(x,y)$ are shown from which $\alpha_{B2}(x,y)$ is determined, as

$$\alpha_{B2}(x,y) = \gamma(x,y) - \delta(x,y)$$

These two angles can be expressed as

$$\gamma(x,y) = \tan^{-1}\left(\frac{x}{y}\right)$$

and

$$\delta(x,y) = \tan^{-1}\left(\frac{x-\Delta w}{y}\right)$$

permitting the second term in the brackets in Eq. (III-1), denoted as T_2, to be written as

$$T_2 = \int_0^h \int_{\Delta w}^w \left[\tan^{-1}\left(\frac{x}{y}\right) - \tan^{-1}\left(\frac{x-\Delta w}{y}\right)\right] dx \, dy$$

Using the same set of identities used to evaluate T_1, the term T_2 can be evaluated as

$$T_2 = \frac{(w-\Delta w)^2}{2} \ln\left(1 + \frac{h^2}{(w-\Delta w)^2}\right) - \frac{h^2}{2} \ln\left(1 + \frac{(w-\Delta w)^2}{h^2}\right)$$

$$+ 2(w-\Delta w)h \cot^{-1}\left(\frac{h}{w-\Delta w}\right)$$

The probability $p_c(\Delta w)$ can then be written in terms of T_1 and T_2, as

$$p_c(\Delta w) = \frac{2}{\pi h w}[T_1 + T_2]$$

which upon combining terms, can be written as

$$p_c(\Delta w) = \frac{h}{2\pi w} \ln\left(\frac{1 + \frac{(w-\Delta w)^2}{h^2}}{1 + \frac{w^2}{h^2}}\right) + \frac{w}{2\pi h} \ln\left(1 + \frac{h^2}{w^2}\right)$$

$$- \frac{(w-\Delta w)^2}{2\pi h w} \ln\left(1 + \frac{h^2}{(w-\Delta w)^2}\right) + \frac{2}{\pi} \cot^{-1}\left(\frac{h}{w}\right)$$

$$- \frac{2(w-\Delta w)}{\pi w} \cot^{-1}\left(\frac{h}{w-\Delta w}\right)$$

Letting

$$r = \frac{h}{w}$$

be defined as the aspect ratio of the pixel, and

$$m_w = \frac{\Delta w}{w}$$

be defined as the fractional pixel misregistration along the scan line $R'(\Delta w)$, or equivalently $R'(m_w)$ can be expressed as

$$R'(m_w) = R\left[1 + \frac{r}{2\pi} \ln\left(\frac{r^2 + (1-m_w)^2}{r^2 + 1}\right) + \frac{1}{2\pi r} \ln(1 + r^2)\right.$$

$$- \frac{(1-m_w)^2}{2\pi r} \ln\left(1 + \frac{r^2}{(1-m_w)^2}\right) + \frac{2}{\pi} \cot^{-1}(r)$$

$$\left. - \frac{2(1-m_w)}{\pi} \cot^{-1}\left(\frac{r}{1-m_w}\right)\right]$$

Using similar arguments $p_c(m_h)$ can be determined in terms of a fractional pixel misregistration between scan lines of m_h, defined as

$$m_h = \frac{\Delta h}{h}$$

and $R'(m_h)$ can be expressed as

$$R'(m_h) = R\left[1 + \frac{1}{2\pi r} \ln\left(\frac{1 + r^2(1-m_h)^2}{1 + r^2}\right) + \frac{r}{2\pi} \ln\left(1 + \frac{1}{r^2}\right)\right.$$

$$- \frac{r(1-m_h)^2}{2\pi} \ln\left(1 + \frac{1}{r^2(1-m_h)^2}\right) + \frac{2}{\pi} \cot^{-1}\left(\frac{1}{r}\right)$$

$$\left. - \frac{2(1-m_h)}{\pi} \cot^{-1}\left(\frac{1}{r(1-m_h)}\right)\right]$$

REFERENCES

1. Holmes, Q. A., "Final MPAD Presentation to LACIE Project Management on LACIE Sample Segment Registration Accuracy", NASA Johnson Space Center Memorandum FM84(75-299), Houston, Tex., 31 Oct 75.

2. Malila, W. A., R. H. Hieber, and R. C. Cicone, Studies of Recognition With Multitemporal Remote Sensor Data, NASA CR-ERIM 109600-19-F, Environmental Research Institute of Michigan, Ann Arbor, Mich., May 1975.

3. Morgenstern, J., R. Nalepka, R. Cicone, J. Sarno, P. Lambeck, and W. Malila, S-192 Analysis: Conventional and Special Data Processing Techniques, NASA CR-ERIM 101900-61-F, Environmental Research Institute of Michigan, Ann Arbor, Mich., September 1975.

4. Gray, H. L., and B. S. Duran, "A Space Application of an Extension of the Buffon Needle Problem", Texas Tech University paper generated under Contract NAS9-12775, not dated.

5. Upensky, J. V., Introduction to Mathematical Probability, McGraw-Hill, New York, 1937, pp. 253-255.

6. Horwitz, H. M., J. T. Lewis and A. P. Pentland, Estimating Proportions of Objects from Multispectral Scanner Data, NASA CR-ERIM 109600-13-F, Environmental Research Institute of Michigan, Ann Arbor, Mich., May 1975.

7. Coberly, W., Serial Correlation of Spectral Measurements, 31 May 1973, NASA:FM8/Mathematics Physics Branch, JSC, Houston, Tex.

8. Cicone, R. C., W. A. Malila, J. M. Gleason, and R. F. Nalepka, "Effects of Misregistration on Multispectral Recognition", to be presented and published in Proceedings of Purdue:LARS Symposium on Machine Processing of Remotely Sensed Data, Lafayette, Ind., Jun 29-Jul 1, 1976.

9. Horwitz, H. M., R. F. Nalepka, P. D. Hyde and J. P. Morgenstern, "Estimating Proportions of Objects Within a Single Resolution Element of a Multispectral Scanner", Seventh International Symposium on Remote Sensing of Environment, Ann Arbor, Mich., May 1971.

10. Rifman, S. S., "Evaluation of Digitally Corrected ERTS Imagery", Proceedings of Symposium on Management and Utilization of Remote Sensing Data, Sioux Falls, South Dakota, Oct. 29 - Nov. 1, 1973, American Society of Photogrammetry, Falls Church, Va.